Z. Kristallogr. **217** (2002) 563–580

© by Oldenbourg Wissenschaftsverlag, München

The crystal chemistry of Mn^{3+} in the clino- and orthozoisite structure types, $Ca_2M_3^{3+}[OH \mid O \mid SiO_4 \mid Si_2O_7]$: A structural and spectroscopic study of some natural piemontites and "thulites" and their synthetic equivalents

K. Langer[I], E. Tillmanns*, [II, III], M. Kersten[I], H. Almen[III] and R. K. Arni[I]

[I] Technische Universität Berlin, Institut für Angewandte Geowissenschaften, D-10623 Berlin, Germany
[II] Universität Wien, Geozentrum, Institut für Mineralogie und Kristallographie, A-1090 Wien, Austria
[III] Universität Würzburg, Institut für Mineralogie, D-97074 Würzburg, Germany

Received July 13, 2001; accepted May 8, 2002

Abstract. Six new structure refinements and eleven sets of polarised, single-crystal electronic absorption spectra, $\mathbf{E} \parallel \mathbf{X}$, $\mathbf{Y}$ and $\mathbf{Z}$, in the energy range 35000–5000 cm^{-1} were obtained on natural and synthetic orthozoisite-type "thulites" and clinozoisite-type piemontites: $Ca_2(Al_{3-p}M_p^{3+})$ $[OH \mid O \mid SiO_4 \mid Si_2O_7]$ where $M^{3+} = Mn^{3+}$ or $(Mn_{1-n}^{3+}Fe_n^{3+})$ for the synthetic or natural minerals, respectively. Electron microprobe analyses of the single crystals studied revealed substitutional degrees $p_{M^{3+}} = 0.13$ or 0.51 in natural and synthetic "thulite", respectively, and $0.57 \leq p_{M^{3+}} \leq 1.17$ or $0.83 \leq p_{M^{3+}} \leq 1.47$ in the natural or synthetic piemontites, respectively.

Manganese in "thulite" is trivalent, as it is in piemontite. In both structure types, M^{3+} fractionates strongly into the axially compressed $[M(3)O_6]$ polyhedra, and does not enter the M(2) sites. Mean M(3)–O and M(1)–O distances increase in both structures, compared to the M^{3+}-free Al end members. Such distance changes in piemontite are +0.47% and +0.53% per $0.1x_{M^{3+}}$, respectively, (x = site fraction). The bending angle of the Si_2O_7-group in cis-configuration, ∢Si(1)–O(9)–Si(2), decreases from 164.4° in clinozoisite to 147.4° in the most Mn^{3+}-rich synthetic piemontite with $p_{Mn^{3+}} = 1.47$ (emp) or $x_{Mn^{3+}(M3)} = 0.931$ and $x_{Mn^{3+}(M1)} = 0.460$ (from structure refinement).

The detailed evaluation of the changes, due to $Al \rightarrow M^{3+}$ substitution, of individual bond lengths, as well as the quantitative evaluation of the intensities of the strong spin-allowed dd bands of Mn^{3+} in M(3), prove that in natural piemontite the preference of Mn^{3+} for M(3) over M(1) is more pronounced than that of Fe^{3+}. This is in accord with the Jahn-Teller effect of $3d^4$-configurated Mn^{3+}. In addition, evaluation of the individual M(3)–O(i) distances with increasing $x_{Mn^{3+}(M3)}$ in piemontite indicates that the axial compression of the $[M(3)O_6]$ polyhedra increases. This contrasts with the behaviour of Fe^{3+}-bearing epidotes and is again in accord with the Jahn-Teller effect of Mn^{3+}.

The polarisation behaviour of the three strong spin-allowed dd-bands of Mn^{3+} in M(3), ν_I at 13000–12000 cm^{-1} ($\mathbf{E} \parallel \mathbf{Y}$), ν_{II} at 19000–18000 cm^{-1} ($\mathbf{E} \parallel \mathbf{Y}$ and $\mathbf{Z}$, $\mathbf{Z} > \mathbf{Y}$) and ν_{III} at 24000–22000 cm^{-1} ($\mathbf{E} \parallel \mathbf{X}$) is best interpreted by assuming a $C_{2v}(C_2'')$ pseudo-symmetry of the M(3) sites, a super-group of their site symmetry C_s. Evaluation of the energies of ν_I, ν_{II} and ν_{III} on the basis of the energy level diagram obtained for Mn^{3+} with the above pseudo-symmetry yields the crystal field parameter 10 Dq = 13540 cm^{-1} for $x_{Mn^{3+}(M3)} = 0.931$. 10 Dq increases slightly by 30 cm^{-1} per $-0.1x_{Mn^{3+}(M3)}$. Such values and the Jahn-Teller splitting of the octahedral crystal-field ground-state of Mn^{3+}, $\delta = \nu_I$, yield a crystal field stabilisation energy of Mn^{3+}(M3) of 14080 cm^{-1} for $x_{Mn^{3+}(M3)} = 0.931$. $CFSE_{Mn^{3+}}$ increases slightly by 28 cm^{-1} per $-0.1x_{Mn^{3+}(M3)}$. Such values are appreciably smaller than those typical of Mn^{3+} substituting for Al in the axially elongated $[M(1)O_6]$ octahedra in the andalusite structure type. This different behaviour of Mn^{3+} in the two structure types is likely due to the smaller deviation of $(c/a)_{oct}$ in piemontite M(3) compared to andalusite M(1) for the same site fractions of Mn^{3+}. In addition, the axial inversion effect – compressed $[M(3)O_6]$ in the clinozoisite-type or elongated $[M(1)O_6]$ in the andalusite-type, involving the electron hole of $3d^4$ in d_{z^2} or $d_{(x^2-y^2)}$, respectively – may play a role.

Introduction

The crystal chemistry and physics of trivalent manganese in minerals and other crystalline materials is greatly influenced by the Jahn-Teller effect (Jahn and Teller, 1937), i.e. by the stabilisation of this $3d^4$-configurated cation in structural sites allowing for a lifting of the degeneracy of the ^5E_g octahedral crystal-field ground state. As a consequence of this effect, the thermodynamic stability range of oxygen-based minerals containing Mn^{3+} substituting for octa-

* Correspondence author
(e-mail: ekkehart.tillmanns@univie.ac.at)

hedrally coordinated spherical ions such as Al or Fe^{3+} is greatly enhanced. The inter- and intracrystalline distributions of Mn^{3+} also do not follow patterns governed by geometrical properties such as polyhedral distances.

These effects were thoroughly studied by structural, spectroscopic and experimental work for octahedral Mn^{3+}–Al substitution in the aluminium silicate minerals (Abs-Wurmbach et al., 1981; 1983). Here, Mn^{3+} partitions nearly exclusively into the andalusite phase, substituting for Al in the strongly elongated M(1) octahedra. This elongation increases significantly with increasing Mn^{3+}-content (Abs-Wurmbach et al., 1981). Such effects lead to a notable expansion of the thermodynamic stability range of the andalusite-type phase at the expense of sillimanite and kyanite (Abs-Wurmbach et al., 1983), which explains the persistence of manganian andalusites far inside the stability field of kyanite, provided the oxygen fugacity of the host rocks was high enough to stabilise trivalent manganese. This behaviour of Mn^{3+} is quite different from that of $3d^5$-configurated, spherical Fe^{3+} when incorporated in phases of the Al_2SiO_5 system (Chinner et al., 1969). The crystal chemical behaviour of Mn^{3+} incorporated in the andalusite structure type has also been confirmed by low temperature electronic spectra on manganian andalusite from Ultevis and on kanonaite from the type locality by Smith et al. (1982). This latter work also included low temperature spectroscopy on piemontite where Mn^{3+} substitutes predominantly for Al in the compressed M(3) octahedra. A small fraction of Mn^{3+} substitutes into M(1) octahedra of the clinozoisite structure type, as revealed by the structure refinement by Dollase (1969) on a crystal from the type locality in Piemont, Italy. The interpretation of the effects of low temperature on the three strong and strongly polarised bands typical of piemontite was based on their assignment of spin-allowed dd-transitions of Mn^{3+} as proposed by Burns and Strens (1967) and later confirmed by a study of synthetic, pure Mn^{3+}-bearing crystals (Langer et al., 1976). Keskinen and Liou (1987) found experimentally that the incorporation of Mn^{3+} in epidote extends the stability field of this phase at high oxygen fugacity, an effect that corresponds to the findings on the behaviour of andalusite. That the compression of the M(3) octahedra in piemontite and the elongation of the M(1) octahedra in andalusite are both compatible with the predictions of the Jahn-Teller theorem and will cause similar effects on the crystal chemistry and physics of both types of minerals compared to their Mn^{3+}-free equivalents was predicted as early as 1966 by Strens.

Pure Mn^{3+}-piemontites, $Ca_2(Al_{3-p}Mn_p^{3+})[OH|O|SiO_4|Si_2O_7]$ with $0.5 \leq p \leq 1.75$, were synthesized as single phase fine-grained material at high pressures and high temperatures in the presence of water and at the oxygen fugacity of the Mn_2O_3/MnO_2 buffer by Anastasiou and Langer (1977). Discontinuities in the lattice constants and refractive indices with respect to composition were observed. However, the partitioning of Mn^{3+} over the different octahedral sites M(1), M(2) and M(3) of the clinozoisite structure type (Dollase 1968) remained unresolved. At a substitutional degree of $p = 0.25$, Mn-bearing orthozoisite was found (Anastasiou and Langer, 1977). In the present paper we use the variety name "thulite" for this phase. So far, it is not proven with certainty, whether Mn is really trivalent in "thulite" or divalent as proposed in most of the literature. Information on the crystal field stabilisation of Mn^{3+} in the clinozoisite type as a function of p is scarce, and that for orthozoisite, when Mn is really trivalent, remains to be determined.

Summarising these introductory remarks, it is obvious that despite the work already done[1], elucidation of the many open questions on crystal chemistry and physics of Mn^{3+} in the clino- and orthozoisite structure types is still necessary. The present study was aimed to fill this gap by studying natural piemontites of different origin, coexisting natural piemontite and "thulite", as well as synthetic piemontites and "thulite" by using high pressure crystal growth methods, electron microprobe analysis, X-ray diffraction structure refinement, and polarised single-crystal electronic spectroscopy.

Materials and methods

Materials

Four natural piemontites, including one coexisting with "thulite", as well as pure synthetic Mn^{3+}-piemontites were studied. The seven synthetic samples were prismatic single crystals with maximum sizes between about 100 and 350 μm, which were produced at high pressures, temperatures and oxygen fugacities in the presence of water. An overview of these materials and the methods by which they were studied is presented in Table 1.

Methods

Crystal growth experiments

on piemontites and "thulite" were performed in a piston-cylinder apparatus at 800 °C and a total pressure of 1.5 GPa using NaCl-based high-pressure cells (Cemič et al., 1990). Run charges plus excess water, as well as the Mn_2O_3/MnO_2 oxygen buffer, were encapsulated in cold-sealed large-volume gold capsules, 4 mm in diameter, and 9 mm long. The capsules had a free volume of about 190 μl and were machined from gold rod. The oxygen buffer was separated from the run charge by a tightly fitting platinum foil in the capsule.

Large single crystals were only obtained when using a method which reduces the nucleation rate by adding one of the components in an oxidation state which slowly transforms during the experiment into that required for the intended phase to grow (Frentrup and Langer, 1981, 1982). Such runs do normally not produce single-phase run products so that crystals have to be picked and need to be chemically analysed as their composition cannot be calculated from the stoichiometry of the starting material.

[1] This includes two notes on our early work in this field (Tillmanns et al., 1984; Kersten et al., 1988).

The starting materials were prepared by intimately mixing ($2\,CaO \cdot 3.23\,SiO_2$)-glass (Anastasiou and Langer, 1977), γ-Al_2O_3 and MnO in proper proportions. Run conditions and products[2] are listed in Table 2.

[2] Among the products of three of the runs quoted in Table 2, small amounts of anhydrite, which formed crystals with dimensions in the 100 µm range, were found, although the starting materials only contained sulfur in the ppm-range at the most. This strange result can only be explained by assuming that sulfur, occurring in traces in the surrounding high-pressure cell, diffused through the wall of the gold capsules, became oxidized to sulfate at the high oxygen fugacity of the buffer and formed anhydrite.

Electron microprobe analyses

were obtained by means of wavelength dispersive measurements using the Cameca Camebax at the ZELMI laboratory of the Technische Universität Berlin. Standards were orthoclase (Si), corundum (Al), wollastonite (Ca, Si), metallic iron (Fe), manganese (Mn) and chromium (Cr), spessartine (Mn), spinel (Mg), albite (Na), rutile (Ti), strontianite (Sr), copper (Cu) and zinc (Zn). Operating conditions were 15 kV and 15 nA with counting times of 20 sec on peak and 10 sec on background. ZAF corrections were performed with the help of the program RSX-14M-plus (version 3.0).

Table 1. "Thulite" and piemontite crystals studied, $Ca_2Al_{3-p}M_p^{3+}[OH \mid O \mid SiO_4 \mid Si_2O_7]$ ($M^{3+} = Mn^{3+}$, Fe^{3+}), by the methods indicated.

	Natural crystals					Synthetic crystals						
Mineral	"Thulite"	Piemontite				"Thulite"	Piemontite					
Term	TUPILA-19	TUPILA-19	PIULT-1	AND-79 255	AND-79 183	MK-25	MK-35	PF-66	MK-40	MK-37	MK-42	MK-41
Source	Lom, Norway	Lom, Norway	Ultevis, Sweden	Andros, Greece	Andros, Greece							
$p_{Mn^{3+}}$ [a]	0.03	0.14	0.66	0.60[b]	0.86	0.51[c]	0.83[c]	0.98[c]	1.06[c]	1.22[c]	1.47[c]	1.48[c]
$p_{Fe^{3+}}$ [a]	0.10	0.43	0.51	0.42	0.18	–	–	–	–	–	–	–
Methods												
Electron microprobe	+	+	+	+	+	+	+	+	+	+	+	+
XRD structure refinement	+	+	+				+	+			+	
Polarised single crystal electronic absorption spectroscopy	+	+	+	+	+	+	+	+		+	+	+

a: cf. Data in Table 4
b: Contains significant amounts of Mn^{2+} [7, 8], such that $Mn_{tot} = 0.82$ pfu (cf. Table 4)
c: $Mn_{tot} = Mn^{3+}$ (cf. Table 4)

Table 2. Conditions and results of synthesis experiments. Starting materials were stoichometric mixtures of a glass ($2\,CaO \cdot 3.23\,SiO_2$), γ-Al_2O_3, MnO plus water according to the general formula $Ca_2Al_{3-p}Mn_p^{3+}[OH \mid O \mid SiO_2 \mid Si_2O_7]$. Oxygen buffered runs, using the $Mn_2O_3 \mid MnO_2$-buffer, were performed in a piston-cylinder apparatus (Cemič et al. 1990) (cf. Text). Abbrevations: Pi = piemontite; Th = "thulite"; Brn = braunite; Qu = quartz; Anhydr. = anhydrite; st = strong; m = medium; w = weak; t = trace.

Run No.	$p_{Mn^{3+}}$ (starting material)	Run conditions			Run products	Piemontite crystals
		T [°C]	p [GPa]	Duration [hrs]		
MK-25	0.6	800	1.50	21.0	Pi, st; Th, st; Brn, t	up to 200 µm, red; Th up to 45 × 150 µm, light red
MK-35	0.8	800	1.50	21.5	Pi, st; Th, m; Brn, w Anhydr., w; Qu, t	up to 200 µm, platy; fragments up to 60 µm thick, dark red
PF-66[a]	1.0	820	1.82	23.0	$(SpessGross)_{ss}$ as ground mass, piem. crystals in the rim of the cake	up to 300 µm, prismatic, dark red
MK-37	1.3	800	1.50	21.5	Pi, st; Th, t; Brn, w; Anhydr., w; Qu, t	up to 200 × 200 µm, platy, 50–60 µm thick; brownish-red
MK-40	1.6	800	1.50	21.0	Pi, st; Anhydr., w; Th, t	250 × 300 µm, platy, 60 µm thick, orange-redbrown
MK-41	1.8	750	1.50	17.0	Pi, st; Brn, w; Qu, w; Anhydr., w; Th, t	400 × 600 µm, platy, 200 µm thick, dark brown
MK-42	2.0	750	1.50	25.0	Pi, st; Brn, w; Th, w; Anhydr., w; Qu, t	300 × 150 µm, platy, 60 µm thick, brown

a: This material was kindly provided by K. R. Frentrup. He obtained it in an experiment to grow large crystals of $(SpessGross)_{ss}$.

Analyses were performed on a number N of spots on the crystals studied. In most cases the standard deviations of the averaged values for the components did not significantly differ from those of repeated measurements on one spot. This indicates that most crystals were homogeneous.

X-ray diffraction and structure refinement

was performed on the "thulite" and piemontite crystals listed in Table 1. Data of structure refinements are presented in Table 3 for inclusion-free, optically clear, hypidiomorphic, prismatic crystals with sizes up to 150 μm, untwinned as checked by microscopic examination and precession photographs. The crystals were mounted on a four-circle single-crystal diffractometer (ENRAF-NONIUS CAD4 (Thu2 to PF66/14, Table 1) or NICOLET R3 (MK42/1, Table 1)) and data were collected in the θ-range 1.0–35.0° by means of $\omega - 2\theta$ or ω-scans (MK42/1) using MoK_a radiation with graphite monochromator.

Lattice constants were calculated by least-squares calculations evaluating the 2θ-values of 25 diffraction spots at high angles. The data were corrected for Lorentz and polarisation effects and linear absorption coefficients were calculated by $(\mu/\varrho) \cdot N_A^{-1}$.

The structure refinements were started using the program SHELX (Sheldrick, 1976), using isotropic temperature parameters, the atom parameters in ortho- and clinozoisite (Dollase 1968) as starting parameters and assuming the octahedral cationic site fractions to be unity. Atomic scattering curves were taken from the International Tables for X-Ray Crystallography vol. IV, (1974). This part of the refinement was continued until the changes of the atomic parameters in the respective cycles were below 2σ. Then, the octahedral site fractions of Al, Mn^{3+} or $(Mn^{3+}{}_{1-n}Fe^{3+}{}_n)$, the latter in the case of natural crystals, (i.e. the cation distribution) were refined with the help of the program RFINE (Finger and Prince, 1975). Finally in a third step the atomic parameters obtained were refined, again with the program SHELX, using anisotropic displacement parameters. Bond length and bond angles in the refined crystal structures were calculated using the program SADIAN (Baur et al., 1986).

Polarised electronic absorption spectra

in the range 35000–5000 cm^{-1} (286–2000 nm) could be obtained at room temperature by means of microscope-spectrometric methods (Langer, 1988) using a Zeiss UMSP 80 equipped with UV-transparent objective and condenser, Ultrafluar 10×, and a Glan-Thompson-type calcite prism polariser. Spectral slit width was 1 nm, the wavelength step width of the grating monochromator was 1 nm. All spectra were obtained averaging 20 I- and I_0-measurements at each step. Entrance and exit apertures had effective diameters of 47 and 25 μm, respectively, in almost all measurements. The reference I_0-spectra were scanned in air.

The crystals were oriented by means of spindle-stage methods and/or X-ray oscillation photographs. Following the orientation, spectra were measured on the platelets with the electrical vector parallel to two of the three axes **X**, **Y** and **Z** of the general refractive index indicatrix (cf. Tröger, 1952). To obtain the spectra with **E** parallel to all three axes of the indicatrix, two differently oriented crystals had to be processed: platelets either $\perp\mathbf{Y}(\|\mathbf{b})$ or $\|\mathbf{Y}(\perp\mathbf{b})$ and, mostly, $\perp\mathbf{X}(\sim\|\mathbf{c})$ were prepared. The optical and crystallographic orientations quoted here were found for the crystals studied by means of conventional microscopic techniques with polarised light as follows

Piemontite: $\mathbf{X}(n_\alpha)$ ca. $\|\mathbf{c}$, yellow – $\mathbf{Y}(n_\beta)$ $\|\mathbf{b}$, violet red – $\mathbf{Z}(n_\gamma) \measuredangle \mathbf{a}$ ($\approx 30°$), carmine
"Thulite": $\mathbf{Z}(n_\gamma)$ $\|\mathbf{c}$, light yellow – $\mathbf{Y}(n_\beta)$ $\|\mathbf{b}$, lilac rose – $\mathbf{X}(n_\alpha)$ $\|\mathbf{a}$ – light greenish.

Table 3. Data for structure refinement of natural and synthetic "thulite" and piemontite.

	Natural crystals			Synthetic crystals		
	"Thulite"	Piemontite		Piemontite		
	TUPILA-19 Thu 2	TUPILA-19 Pie 1	PIULT-1	MK-35/8	PF-66/14	MK-42
$p_{Mn^{3+}}$ [a, b]	0.030	0.143	0.660	0.83[c]	0.98[c]	1.47[c]
$p_{Fe^{3+}}$ [a]	0.096	0.432	0.506	–	–	–
a [Å]	16.2051(37)	8.8739(11)	8.8756(11)	8.847(2)	8.844(1)	8.855(1)
b [Å]	5.5488(12)	5.6156(8)	5.6734(7)	5.674(1)	5.677(1)	5.713(1)
c [Å]	10.0229(18)	10.1484(13)	10.1686(13)	10.170(1)	10.167(1)	10.208(1)
β [°]		115.49	115.50	115.56(1)	115.54(1)	115.62(1)
V [Å^3]	902.1	456.5	462.1	460.6	460.6	465.6
S.G.	*Pnma*	$P2_1/m$	$P2_1/m$	$P2_1/m$	$P2_1/m$	$P2_1/m$
Z	4	2	2	2	2	2
No. of independ. Reflect.	2124	3027	1922	2175	3044	2201
R_w	0.037	0.034	0.047	0.037	0.035	0.048

a: analysed by microprobe (cf. Table 4)
b: $Mn_{tot} = Mn^{3+}$
c: the crystals used in the X-ray refinement are assumed to have the same composition as those analyzed (Table 4)

This is in accordance with orientations quoted by Tröger (1952). Some of the crystals, especially synthetic crystals with high $p_{Mn^{+3}}$, were twinned ||(100). In such cases, the crystals were oriented such that the twin lamellae were perpendicular to the platelets. The lamellae were wide enough to allow for the microscope-spectrometric measurements. The orientation of the linearly polarised measuring radiation **E** || **X**, ||**Y** and ||**Z** was fixed for all crystal platelets in the green region at about 20000 cm^{-1}.

The platelets were embedded in resin, together with a quartz ||[0001] and a diaspore (010) platelet which served in the thickness measurement by their retardation. The mounts were ground and polished from both sides to obtain platelets with suitable thickness according to band intensities such that all band maxima were below absorbance values of 3. To record weak bands as well as strong ones with reliability, it was necessary for some of the samples to start with a thick crystal slide, which after the first measurement was further thinned down and scanned again. Thicknesses of the plates used in the spectral scannings were in the range $10 \leq t\,[\mu m] \leq 28$. All spectra obtained on the various crystal plates prepared were recalculated for a thickness of 1 cm, thus the spectra ordinate is always the linear absorption coefficient $\alpha = \log(I_0/I)/t$ in [cm^{-1}].

Results and discussion

Chemical composition of the crystals

Table 4 compiles the data on chemical composition of the "thulite" and piemontite single crystals studied. The electron microprobe results were recalculated to obtain the numbers of cations (±1esd) per 25 negative charges of the formula units. Generally, total Mn was calculated as Mn^{3+} (Table 4, b). This procedure may seem to be doubtful at least in the case of "thulite", in which Mn is proposed to

Table 4. Results of electron microprobe analyses of natural and synthetic "thulite" and piemonite crystals studied. The results of measurements on N different spots, including those of spectral measurements, were recalculated to number of ions per 25 negative charges of the formula unit and then averaged. Standard deviations, 1σ, are given in parentheses. Generally total manganese was calculated as Mn^{3+} (b). In case of some crystals, this procedure yielded an octahedral population with significant excess of (M1 + M2 + M3) over 3.00 and an (A1 + A2)-population below 2.00. This indicates that a fraction of Mn is divalent. In such cases, the analyses were recalculated to the respective amounts of Mn^{3+} and Mn^{2+} (a). Deviations up to 0.05 from 3.00[6] or 2.00[7, 8], are within the error of analyses and were not subjected to the recalculations of type (a). (c) The $\Sigma_{[6]}$ was calculated for Mn in the different valence states (a).

	N	(A1 + A2)						(M1 + M2 + M3)						(Si1 + Si2 + Si3)
		Ca	Sr	Mg	Mn^{2+} (a)	Zn	$\Sigma_{[7,8]}$	Al	Mn^{3+} (a)	Mn^{3+} (b)	Fe^{3+}	Cu	$\Sigma_{[6]}$	
Natural crystals														
"Thulite"														
TUPILA 19 Thu 2		1.97	<0.01	<0.01	–	0.01	1.98	2.86	–	0.03	0.10	0.01	3.00	3.02
Piemontite														
TUPILA 19 Pie 1		1.98	<0.01	<0.01	–	0.01	1.99	2.43	–	0.14	0.43	0.01	3.01	2.99
PIULT 1	3	2.00	–	–	–	–	2.00	1.87	–	0.66	0.51	–	3.04	2.97
AND 79–183 Pie 7	14	1.89(3)	0.08(3)	–	–	–	1.97	1.96(4)	–	0.90(4)	0.16(2)	–	3.02	3.01(2)
Pie 14	10	1.92(4)	0.05(3)	–	–	–	1.97	1.93(4)	–	0.86(2)	0.21(3)	–	3.00	3.02(2)
AND 79–255 Pie 2	7	1.76(4)	<0.01(3)	–	0.23(4)	–	1.99	1.97(4)	0.59(3)	0.81(3)	0.41(2)	–	2.97[c]	2.97(1)
Pie 4	17	1.74(7)	<0.01(3)	–	0.25(6)	–	1.99	1.96(5)	0.60(3)	0.84(6)	0.42(4)	–	2.99[c]	2.97(1)
Synthetic crystals														
"Thulite"														
MK 25 Thu 1	16	1.98(1)	–	–	0.06(2)	–	2.04	2.55(5)	0.44(4)	0.50(4)	–	–	2.99	2.97(1)
Thu 4	17	1.97(1)	–	–	0.08(1)	–	2.05	2.54(5)	0.45(4)	0.53(4)	–	–	2.99	2.97(1)
Piemontite														
MK 35 Pie 24	20	1.92(1)	–	–	0.11(2)	–	2.03	2.26(5)	0.73(5)	0.83(4)	–	–	2.99	2.97(2)
PF 66 Pie 1	4	1.98(2)	–	–	–	–	1.98	2.01(1)	–	1.00(3)	–	–	3.01	3.00(2)
Pie 2	7	1.92(3)	–	–	–	–	1.92	2.09(3)	–	0.95(4)	–	–	3.04	3.01(2)
MK 40 Pie 2	16	1.98(2)	–	–	–	–	1.98	1.93(6)	–	1.11(6)	–	–	3.04	2.98(1)
Pie 6(I)	8	1.98(2)	–	–	–	–	1.98	2.02(2)	–	1.01(2)	–	–	3.03	3.00(2)
MK 37 Pie 13	14	1.96(1)	–	–	–	–	1.96	1.82(6)	–	1.23(4)	–	–	3.05	2.99(2)
Pie 2	19	1.98(2)	–	–	–	–	1.98	1.83(11)	–	1.21(8)	–	–	3.04	2.99(2)
MK-42 Pie 6	19	1.97(1)	–	–	–	–	1.97	1.59(4)	–	1.45(3)	–	–	3.04	2.98(1)
Pie 8	14	1.97(2)	–	–	–	–	1.97	1.55(3)	–	1.48(4)	–	–	3.03	2.99(1)
MK-41 Pie 5(II)	27	1.97(2)	–	–	–	–	1.97	1.65(6)	–	1.39(4)	–	–	3.04	2.99(2)
Pie 6	19	1.93(2)	–	–	–	–	1.93	1.47(5)	–	1.57(4)	–	–	3.04	3.01(1)

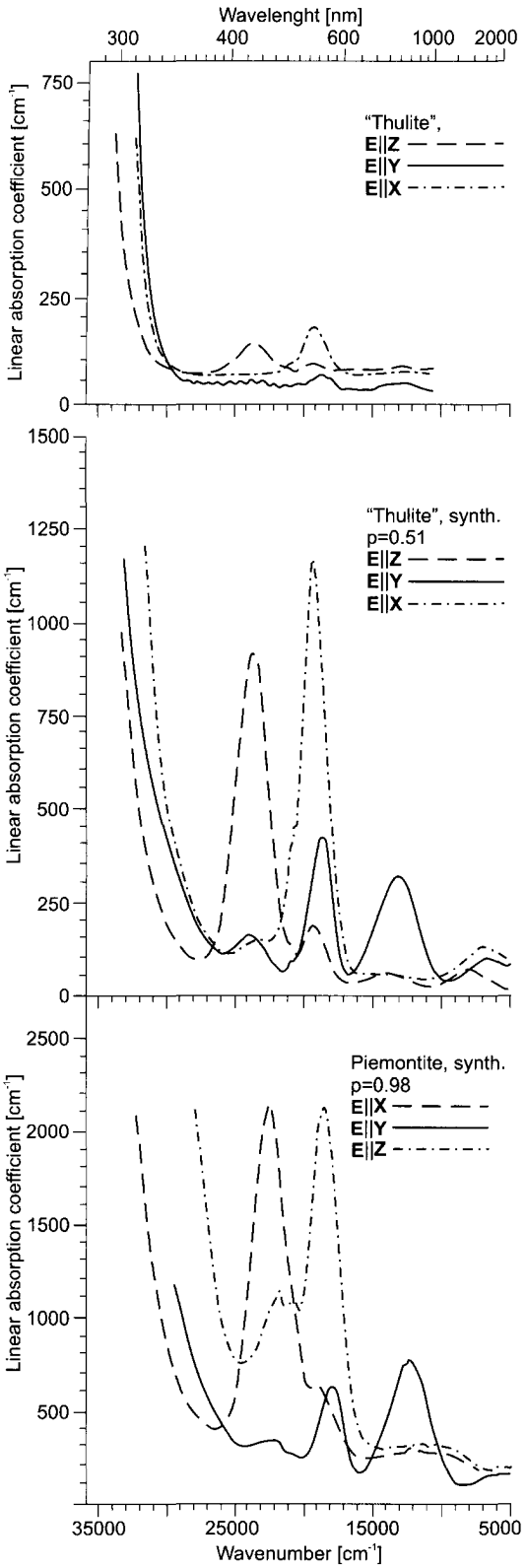

Fig. 1. Polarised electronic absorption spectra of "thulite" from Lom, TUPILA-19/Thu 21 (plate $\perp$**Y**, **b**: measurement with **E** || **X** and **E** || **Z**) and /Thu 11 (plate $\perp$**Z**, **c**: measurement with **E** || **Y**), synthetic "thulite" MK-25/Thu 1 (plate $\perp$**Y**, **b**: measurement with **E** || **X** and **E** || **Z**) and /Thu 4 (plate $\perp$**X**, a: measurement with **E** || **Y**) and synthetic piemontite PF-66/Pie 1 (plate $\perp$**Y**, **b**: measurement with **E** || **X** and **E** || **Z**) and /Pie 2 (plate $\perp$**X**, $\sim$ **c**: measurement with **E** || **Y**). The comparison of the intense bands, which are caused by dd-transitions of Mn^{3+} in the case of piemontites (Burns and Strens, 1967; Langer et al.,1976) proves that manganese is trivalent also in the orthozoisite-type "thulite".

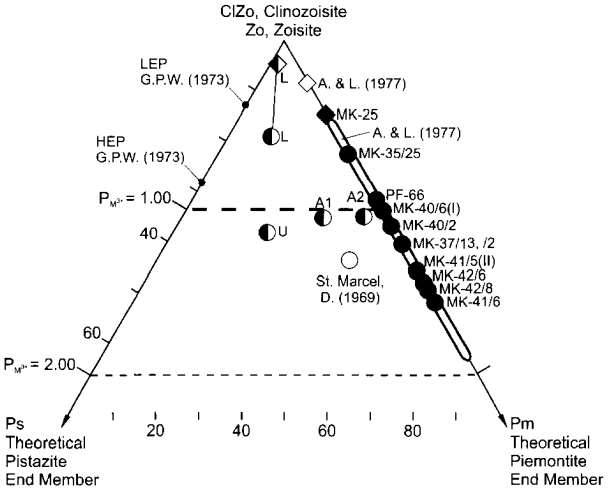

Fig. 2. Composition of "thulites" and piemontites studied, represented schematically in the triangular compositional diagram spanned by the theoretical end members Zo/ClZo ($Ca_2Al_3Si_3O_{10}OH$), Ps ($Ca_2Fe_3^{3+}Si_3O_{10}OH$), and Pm ($Ca_2Mn_3^{3+}Si_3O_{10}OH$). Symbols: circles = piemontites, diamonds = "thulites", full symbols = synthetic, pure Mn^{3+} -bearing solid solutions, half filled symbols = natural minerals, open symbols and open beam on the ClZo/Zo – Pm edge = related literature data; A1 and A2 samples from Andros (AND79–255, AND79–183), L = Lom, U = Ultevis; A. & L. (1977) = Anastasiou and Langer (1977), D. (1969) = Dollase (1969). The numbers of the synthetic crystals refer to Table 1.

be divalent by many authors (cf. e.g. Strunz, 1978). However, the polarised single crystal spectra of natural "thulite", synthetic "thulite" and pure Mn^{3+}-bearing piemontite (Fig. 1) exhibit the same strong bands, which were previously proven to originate from Mn^{3+} (see introduction), so there is no doubt about the trivalent state of Mn in "thulite", and about colour and pleochroism of this mineral being caused by Mn^{3+}.

On the other hand, calculating total Mn as Mn^{3+} yields a slight excess of $\Sigma_{[6]}$ over 3.00 pfu and a concomitant deficiency of $\Sigma_{[7,8]}$ in synthetic "thulite", MK-25/Thu1 and Thu4, as well as a significant excess in natural or synthetic piemontite crystals AND79–255/Pie2 and Pie 4 or MK-35/Pie 24. In these cases, total Mn was recalculated to Mn^{3+} and Mn^{2+} to achieve cationic sums close to the optimised $\Sigma_{[6]} = 3.00$ and $\Sigma_{[7,8]} = 2.00$ (Table 4). It is obvious that in the natural piemontite AND79–255, a significant fraction of the [7,8]-coordinated A-sites is occupied by Mn^{2+}, $x_{Mn^{2+}[7,8]} = 0.12$ (cf. Table 4); this cation being also present in the two afore-mentioned synthetic "thulite" crystals from run MK-25 and in one piemontite crystal, but with lower site fractions of $x_{Mn^{2+}[7,8]} = 0.04$ and 0.06 respectively.

Where analyses of two crystals are quoted in Table 4, the two individual crystals used for the spectroscopic measurements were analysed. In all these cases, except for MK-41/Pie5(II) and /Pie6, the data on cations pfu differ by less that $\pm$1esd. Even in this latter case, the differences are not so great that they would cause significant differences in Mn^{3+} dd-band intensities in the electronic spectra of this specimen. This allows the analysis of only one crystal to be representative for the respective specimen (TUPILA-19/Thu2, /Pie1, PIULT-1). The values of esd of Al and Mn^{3+} in the synthetic piemontite crystal MK-37/

Pie 2 are twice as high as for the other crystals and for repeated analyses on one spot. This indicates that the crystal is slightly inhomogeneous.

The Cu and Zn contents of the coexisting minerals from Lom (Table 4) are notable, but are so low that they will not influence the Mn related properties analysed here.

The compositions of the crystals studied are plotted in Fig. 2, which illustrates convincingly the fact that maximum Mn^{3+}-contents in piemontite, ca. 1.5 pfu in this study, are appreciably higher than the maximum Fe^{3+}-contents in epidotes, which are ca. 1.1 pfu. Furthermore, it is obvious that in coexisting "thulite" and piemontite, Mn and Fe partition predominantly into the latter phase.

Refractive indices and lattice constants in dependence on the substitutional degrees $p_{Mn^{3+}}$ for synthetic, or $p_{M^{3+}}$ with $M^{3+} = (Mn^{3+}{}_{1-n}Fe^{3+}{}_n)$, for natural crystals

Fig. 3 displays the refractive indices measured on crystals of the synthetic Al–Mn^{3+} "thulite" and piemontites, $Ca_2(Al_{3-p}Mn_p^{3+})[OH\,|\,O\,|\,SiO_4\,|\,Si_2O_7]$, as a function of the substitutional degree $p_{Mn^{3+}}$. All three refractive indices increase with increasing Mn content, though with slightly different slopes; $dn/dp_{Mn^{3+}}$ being highest parallel **Z** and lowest parallel **X**. There are no indications of discontinuities in the range of $p_{Mn^{3+}} = 1$ (Fig. 3) where the substituted position might be expected to change. Such breaks were thought to exist in plots obtained from measuring very fine-grained synthetic piemontites (Anastasiou and Langer, 1977). These measurements, shown as dashed lines in Fig. 3, were subject to large errors at least parallel

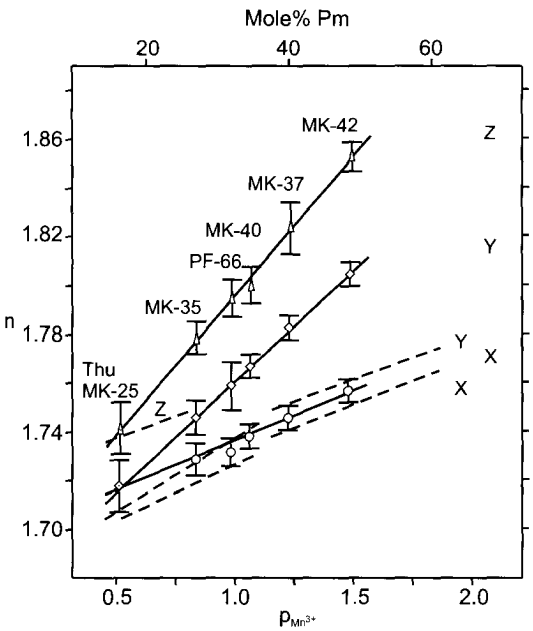

Fig. 3. Refractive indices, n_α ($\|\,\mathbf{X}$), n_β($\|\,\mathbf{Y}$) and n_γ ($\|\,\mathbf{Z}$), of synthetic Al–Mn^{3+}-"thulite" and piemontite as a function of composition. Data of this study (solid lines) are shown in comparison with those of Anastasiou and Langer (1977) which were obtained on very small crystals with lengths up to 40 μm (broken lines). Due to uncertainties resulting from small crystal size, the earlier data obtained $\|\,\mathbf{Y}$ are definitely incorrect.

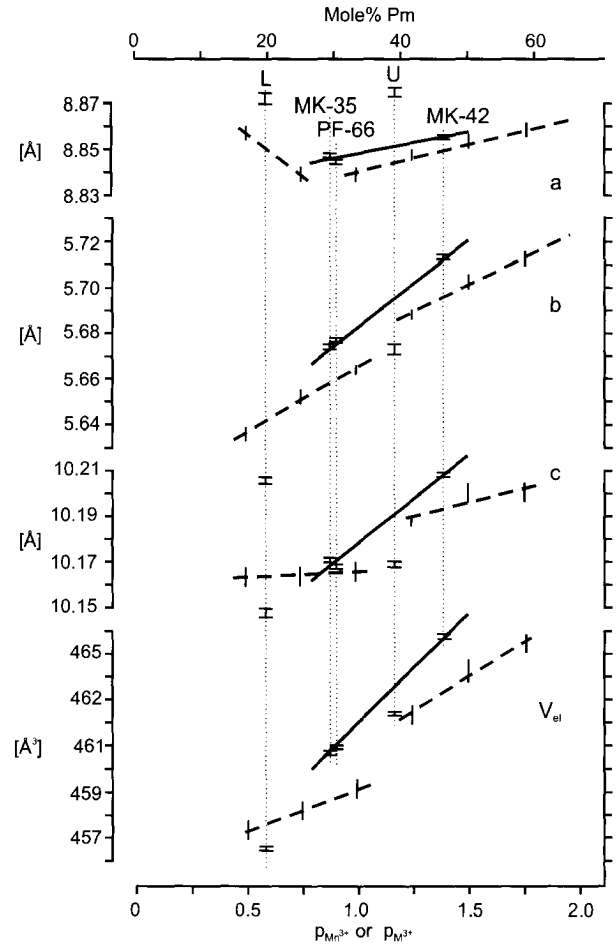

Fig. 4. Lattice constants and unit cell volumes of synthetic Al–Mn^{3+}-piemontites as a function of composition in terms of the substitutional degree $p_{Mn^{3+}}$. Data of this study (solid lines and data connected by thin, dotted vertical lines) are shown in comparison with those of Anastasiou and Langer (1977) (broken lines and data represented by |). The data on natural, $(Mn^{3+}{}_{1-n}Fe^{3+}{}_n)$-substituted piemontites from Lom, L, and Ultevis, U, are also shown. These were plotted over $p_{Mn^{3+}} = Mn^{3+} + Fe^{3+}$. The data obtained in the present work are taken from Table 3.

to **Y** and parallel to **Z** due to small crystal sizes as is obvious from the plots.

Fig. 4 displays the lattice constants of the three structurally refined synthetic piemontites MK-35/8, PF-66/14 and MK-42/1, as well as those of the two refined natural piemontites from Lom (L) and from Ultevis (U) (cf. Table 1) as a function of $p_{Mn^{3+}}$ or $p_{M^{3+}}$, with $M^{3+} = (Mn^{3+}{}_{1-n}Fe^{3+}{}_n)$. Again, these data and their p-dependent slopes are compared with earlier results on fine-grained synthetic piemontites (Anastasiou and Langer, 1977). The earlier results are in approximate agreement with the present data, when the errors of both data sets are considered. However, the breaks postulated previously near $p = 1$ are not confirmed, except maybe for $a = f(p)$. The reason may be that the single crystal data are too few and also are lacking in the critical range close to $p = 1$. Further, it may be debated as to whether or not the spherically symmetrical $3d^5$-configurated Fe^{3+} has the same effect on the lattice constants as the $3d^4$-configurated Mn^{3+} with its peculiar crystal chemical properties; an assumption that is inferred when summing up $p_{M^{3+}} = Mn^{3+} + Fe^{3+}$.

Most significant structural changes on increasing Mn^{3+}- or M^{3+}-contents, intracrystalline cation distribution and interatomic distances

This section presents the significant structural properties and changes in the zoisite and clinozoisite structure types on increasing substitutions $Al \rightarrow Mn^{3+}$ or $Al \rightarrow (Mn^{3+}{}_{1-n}Fe^{3+}{}_n)$ as revealed by the study of the synthetic or natural crystals (cf. Table 1), respectively. We do not list all the structural data obtained (i.e. all atom parameters, isotropic and anisotropic displacement parameters, all interatomic distances and angles) for the set of the six different crystals studied. This is justified because all structural properties aside those presented here remain virtually unchanged on changing substitutional degree.

The structures of the clino- and orthozoisite-types contain the following octahedral positions per formula unit (Dollase, 1968) where Al and M^{3+} may be allocated:
Clinozoisite-type, SG $P2_1/m$, $Z = 2$:
1 M(1), Wyckoff site 2a, site symmetry $\bar{1}$: edge connected octahedra forming straight, single chains $\|\mathbf{b}$
1 M(2), Wyckoff site 2c, site symmetry $\bar{1}$: edge connected octahedra forming straight, single chains $\|\mathbf{b}$
1 M(3), Wyckoff site 2e, site symmetry m: octahedra attached on alternating sides of the M(1)-chain by edge connection.
Zoisite-type, SG *Pnma*, $Z = 4$:
2 M(1, 2), Wyckoff site 8d, site symmetry 1: edge connected octahedra forming straight, single chains $\|\mathbf{b}$
1 M(3), Wyckoff site 4c, site symmetry m: octahedra attached on one side of the M(1, 2)-chain by edge connection.

Fig. 5 shows the different octahedra in the clinozoisite-type projected onto the (010) plane. The orientations and values of the lattice constants, a and c, occurring in this plane, the orientation of the two main optical directions **X** and **Z**, as well as the internal octahedral axes of the M(3) octahedron to be discussed in the spectroscopy section, are also shown.

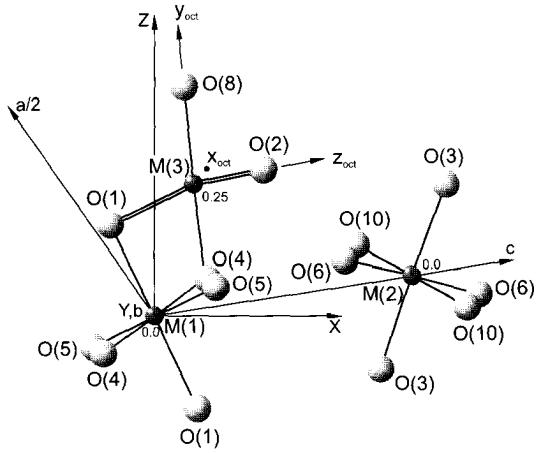

Fig. 5. The three different octahedra M(1), M(2) and M(3) in the clinozoisite structure type projected along the **b**-axis onto the (010) plane. The orientations of the crystallographic **a**- and **c**-axes as well as that of the principal axes of the optical indicatrix **X**, **Y** and **Z** (Tröger, 1952) and the internal octahedral axes of the M(3) octahedron under the $C_{2v}(C_2'')$ pseudo-symmetry applied in the assignment of spin-allowed dd-bands of Mn^{3+}(M3) are also shown. The figure is produced using the structure data of Dollase (1968) on clinozoisite. The labelling of oxygen atoms of this paper is used.

The present structure refinements of the $Ca_2(Al_{1-p}M_p^{3+})[OH \mid O \mid SiO_4 \mid Si_2O_7]$ phases were performed on three synthetically grown, pure Al–Mn^{3+}-piemontites with substitutional degrees of $p_{M^{3+}} = 0.83$, 0.98 and 1.47 Mn^{3+} (Table 1) and on one natural "thulite" as well as two natural piemontites with $p_{M^{3+}} = 0.13$, and 0.57 or 1.17 $(Mn^{3+}{}_{1-n}Fe^{3+}{}_n)$, respectively (Table 1). The

Table 5. Cation occupancies of M(1), M(2) and M(3) sites in "thulite" and piemontites as revealed by structure refinements of natural and synthetic crystals (cf. Tables 1, 3 and 4). Piemontite from St. Marcel (Dollase, 1969) is included for comparison.

		Natural "thulite"	Natural piemontite			Synthetic piemontite		
		Lom Thu 2	Lom Pie 1	PIULT-1	St. Marcel (Dollase 1968)	Mk-35/8	PF-66/14	MK-42/1
M(1, 2)	Al	0.995						
	M^{3+}	0.005						
	$M_{1,2}{}^{3+}/M_{tot}{}^{3+}$	0.036						
M(1)	Al		0.951	0.844	0.800	0.832(7)	0.827(6)	0.540(7)
	M^{3+}		0.049	0.156	0.200	0.168(7)	0.173(6)	0.460(7)
	$M_1{}^{3+}/M_{tot}{}^{3+}$		0.086	0.136	0.194	0.191	0.190	0.330
M(2)	Al		0.978	0.974	1.000	1.000	1.000	1.000
	M^{3+}		0.022	0.026	0.000	0.000	0.000	0.000
	$M_2{}^{3+}/M_{tot}{}^{3+}$		0.039	0.023	0.000	0.000	0.000	0.000
M (3)	Al	0.867	0.499	0.036	0.170	0.285(8)	0.260(7)	0.069(8)
	M^{3+}	0.133	0.501	0.964	0.830	0.715(8)	0.740(7)	0.931(8)
	$M_3{}^{3+}/M_{tot}{}^{3+}$	0.964	0.881	0.841	0.806	0.810	0.810	0.670
$M_{tot}{}^{3+}$	Refinement	0.139	0.572	1.146	1.030[a]	0.883	0.913	1.391
	emp-analysis	0.130	0.575	1.166	1.030	0.830	0.980	1.470
M^{3+}-type	emp-analysis	$(Mn^{3+}_{0.23}Fe^{3+}_{0.77})$	$(Mn^{3+}_{0.25}Fe^{3+}_{0.75})$	$(Mn^{3+}_{0.56}Fe^{3+}_{0.44})$	$(Mn^{3+}_{0.7}Fe^{3+}_{0.3})$	Mn^{3+}	Mn^{3+}	Mn^{3+}

a: The emp-analysed value was used as constraint in the refinement

most significant changes are the octahedral site fractions of Al and M^{3+} and from these the intracrystalline M^{3+} cation distribution, as well as the related interatomic bond lengths and their changes with the substitutional degree $p_{M^{3+}}$. Also, the Si(1)–O(9)–Si(2) angle changes considerably with $p_{M^{3+}}$.

From the Mn^{3+} and Fe^{3+} contents per formula unit analysed in the natural minerals (Table 4), their respective binary fractions are calculated as ($Mn_{0.23}{}^{3+}Fe_{0.77}{}^{3+}$) for "thulite" from Lom, ($Mn_{0.25}{}^{3+}Fe_{0.75}{}^{3+}$) for piemontite from Lom, and ($Mn_{0.56}{}^{3+}Fe_{0.44}{}^{3+}$) for piemontite from Ultevis (Table 5). As the X-ray scattering curves of Mn^{3+} and Fe^{3+} are so similar, the two cations could not be discriminated in the refinements. Thus the results on site occupancies, cation distribution and distance changes refer to the "averaged cations" just mentioned. It is obvious that the "dilution" of Mn^{3+} by Fe^{3+} in the natural minerals will reduce any special effects of Mn^{3+} caused in the structures by the peculiar electronic properties of this $3d^4$ cation (the Jahn-Teller effect). In turn, any significant difference in the data and their $p_{M^{3+}}$-dependence on $M^{3+} = Mn^{3+}$ compared to $M^{3+} = (Mn_{1-n}{}^{3+}Fe_n{}^{3+})$ indicates this effect in the structures studied.

Site fractions and intracrystalline distribution of Al and M^{3+}

The site fractions of Al and M^{3+} as revealed by the crystal structure refinements are presented in Table 5. Data on piemontite from St. Marcel (Dollase, 1969) are included for comparison with those on the Ultevis piemontite. This may be of interest as both minerals are close in their substitutional degree $p_{M^{3+}}$, the former, however, having a significantly higher Mn^{3+} fraction (Table 5). Table 5 shows that in all cases M^{3+} is strongly enriched on the M(3) site but does not reach $x_{M^{3+}} = 1$ even at a substitutional degree well above 1 (Table 6, $p_{M^{3+}} = 1.47$ in MK-42/1). Quite opposite to the occupancy of the M(3) site, the M(2) octa-

Table 6. Some interatomic distances [Å] and the Si(1)–O(9)–Si(2) angle of the Si_2O_7-group in natural and synthetic "thulite" and piemontites (cf. Tables 1, 3 and 4). Data on ortho- and clinozoisite of Dollase (1968) and of piemontite from St. Marcel (Dollase 1969) are quoted for comparison. Atomic labelling according to Dollase (1968).

	Zoisite	"Thulite"	Clinozoisite	Piemontites					
	(Dollase 1968)	Lom Thu 2	(Dollase 1968)	Lom Pie 1	Ultevis PIULT-1	St. Marcel (Dollase 1968)	Mk-35/8	PF-66/14	MK42/1
$p_{M^{3+}}$	0.09	0.130	0.03	0.57	1.17	1.03			
$p_{M^{3+}}$							0.83	0.98	1.47
Distances									
Ca(1)–O(average)	2.461	2.463	2.467	2.478		2.468	2.464	2.463	2.467
Ca(2)–O(average)	2.609	2.605	2.594	2.579		2.603	2.587	2.589	2.602
Si(1)–O(average)	1.635	1.625	1.625	1.633		1.629	1.625	1.625	1.622
Si(2)–O(average)	1.611	1.613	1.615	1.623		1.620	1.615	1.617	1.622
Si(3)–O(average)	1.650	1.641	1.644	1.648		1.644	1.635	1.638	1.637
M(1,2)–O(1)	1.963	1.980(2)	–	–	–	–	–	–	–
M(1,2)–O(3)	1.849	1.853(2)	–	–	–	–	–	–	–
M(1,2)–O(4)	1.839	1.835(2)	–	–	–	–	–	–	–
M(1,2)–O(5)	1.901	1.900(2)	–	–	–	–	–	–	–
M(1,2)–O(6)	1.927	1.927(2)	–	–	–	–	–	–	–
M(1,2)–O(10)	1.849	1.839(2)	–	–	–	–	–	–	–
M(1,2)–O (average)	1.888	1.889	–	–	–	–	–	–	–
M(1)–O(1) 2*x*	–	–	1.930	1.928(1)	1.945(2)	1.941(4)	1.935(1)	1.939(1)	1.973(1)
M(1)–O(4) 2*x*	–	–	1.850	1.866(1)	1.865(2)	1.872(5)	1.872(2)	1.867(1)	1.882(2)
M(1)–O(5) 2*x*	–	–	1.936	1.966(1)	1.976(2)	1.985(5)	1.971(2)	1.974(2)	2.014(2)
M(1)–O (average)	–	–	1.906	1.920	1.929	1.932	1.926	1.927	1.956
M(2)–O(3) 2*x*	–	–	1.859	1.853(1)		1.857(4)	1.855(2)	1.854(1)	1.856(2)
M(2)–O(6) 2*x*	–	–	1.923	1.944(1)		1.934(5)	1.940(2)	1.935(1)	1.944(2)
M(2)–O(10) 2*x*	–	–	1.852	1.881(1)		1.881(6)	1.877(2)	1.878(1)	1.889(2)
M(2)–O (average)	–	–	1.878	1.893		1.891	1.891	1.889	1.896
M(3)–O(1) 2*x*	2.133	2.122(2)	2.184	2.234(1)	2.257(3)	2.274(5)	2.272(2)	2.269(2)	2.277(3)
M(3)–O(2) 2*x*	1.964	1.960(2)	1.926	1.991(1)	2.018(3)	2.031(5)	2.020(3)	2.019(2)	2.045(3)
M(3)–O(4)	1.821	1.837(3)	1.861	1.898(1)	1.913(3)	1.900(6)	1.872(2)	1.875(2)	1.886(2)
M(3)–O(8)	1.784	1.778(3)	1.781	1.815(1)	1.866(3)	1.861(6)	1.824(3)	1.832(2)	1.851(3)
M(3)–O(average)	1.966	1.963	1.977	2.027	2.055	2.062	2.047	2.047	2.063
Angle									
Si(1)–O(9)–Si(2)	172.6(8)		164.3(5)	157.4(1)	150.6(1)		151.0(2)	149.6(2)	147.4(2)

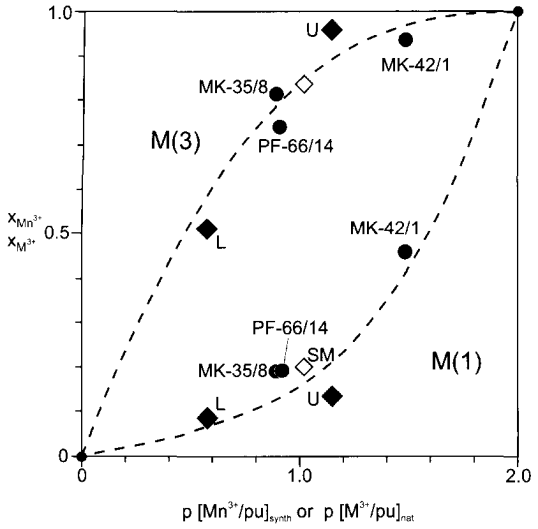

Fig. 6. Intracrystalline distribution of cations between the octahedral M(3) and M(1) sites in the structure of piemontites. In case of natural piemontites (diamonds), the distribution of $M^{3+} = (Mn^{3+}{}_{1-n}Fe^{3+}{}_n)$ is plotted, that of Mn^{3+} in case of pure, synthetic Mn^{3+}-bearing crystals (circles). Open and closed symbols: data from Dollase (1969) and from this study, respectively. The site fractions are designated as $x_{Mn^{3+}}$ + or $x_{M^{3+}}$.

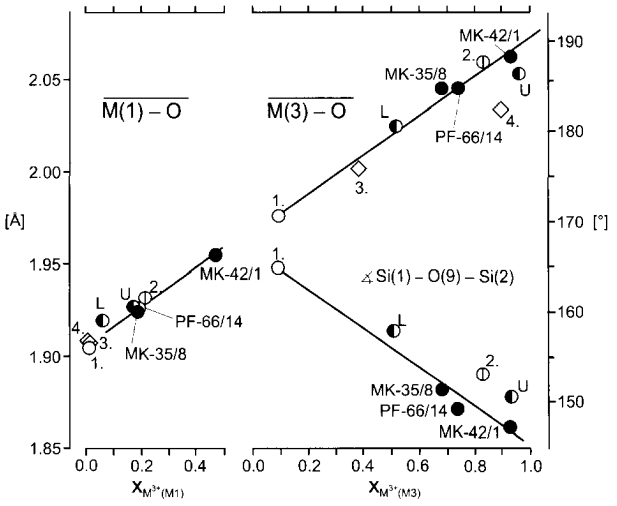

Fig. 7. Mean metal-oxygen distances in M(1) and M(3) octahedra and Si–O–Si angle of the cis-oriented Si_2O_7 groups in the structure of piemontites as a function of the respective site fractions $x_{M^{3+}}$, where $M^{3+} = Mn^{3+}$ in pure synthetic manganese piemontites or $(Mn^{3+}{}_{1-n}Fe^{3+}{}_n)$ in natural manganese and iron bearing piemontites. The literature data for clinozoisite (1.) (Dollase, 1968), piemontite from St. Marcel (2.) (Dollase, 1969) as well as for low-iron (3.) and high-iron epidote (4.) (Gabe et al., 1973, Si–O–Si angles are not quoted by these authors) are also shown. Fully and half closed symbols represent data of this work (cf. Table 6, L = Lom, U = Ultevis).

hedron carrying the protons bound to its cis-standing O(10) atoms allocates if ever any, only very small parts of the M^{3+} pfu, present in the respective samples: ca. 2% or 3% in the Lom or Ultevis piemontites, respectively. If this is really significant compared to the other refined piemontites, it may be due to the fact that in the piemontites from Lom and Ultevis the fraction of Fe^{3+} is high compared to all others (Table 5). The fraction of total $p_{M^{3+}}$ allocated in the centrosymmetric M(1) site, is in all cases smaller than that allocated in M(3). With raising substitutional degree $p_{M^{3+}}$ this M(1)-site fraction increases, most sharply above $p_{M^{3+}} = 1$.

The M^{3+} site fractions of Table 5 for M(3) and M(1) in piemontites are plotted in the distribution diagram of Fig. 6 as a function of total M^{3+} contents, where $M^{3+} = Mn^{3+}$ or $(Mn_{1-n}{}^{3+}Fe_n{}^{3+})$ in synthetic or natural piemontites, respectively. This procedure seems to be a bit daring as the intracrystalline cation distribution is dependent on the growth temperature of the minerals. However, the fractionation of M^{3+} into M(3) is so strong that an effect of a temperature difference between natural and synthetic crystals of about 200 °C will not greatly change the general distribution pattern. It is obvious from Fig. 6 that there is no difference in the distribution behaviour of M^{3+}, be it Mn^{3+} or $(Mn_{1-n}{}^{3+}Fe_n{}^{3+})$, that could account for the special electronic properties of the trivalent manganese.

Interatomic distances and values of the bending angle of the Si_2O_7 group

Data on distances and angles that change significantly on increasing $Al \rightarrow M^{3+}$ substitution, are presented in Table 6. The mean metal oxygen distances in the M(1) and M(3) octahedra and the Si(1)–O(9)–Si(2) angle are plotted as a function of the site fractions $x_{M^{3+}}$ of M(1) or M(3) of the piemontite solid solutions of this work and of that in piemontite from St. Marcel in Fig. 7. The slope of the linear functions in Fig. 7 is defined using the respective data for clinozoisite (Dollase, 1968) as the reference where $x_{M^{3+}}$ equal or close to zero.

The slope $\Delta\bar{R}_{M-O}/\Delta x_{M^{3+}}$ is nearly the same for M(1) and M(3), $\bar{R}_{M-O}$ being larger for M(3) than for M(1) by 3.4% along the linear function, up to $x_{M^{3+}} \approx 1.0$, in M(3). This significant difference in the mean $\bar{R}_{M-O}$ of M(1) and M(3) is obviously one of the reasons for the facts that Mn^{3+} fractionates predominately into the latter site and that the substitution $Al \rightarrow Mn^{3+}$ proceeds up to a site fraction of about 0.5 only in the former. Otherwise, local strains in the structure would be too high. The bending angle of the cis-orientated Si_2O_7 group, ∢ Si(1)–O(9)–Si(2), decreases by about 10% on increasing $Al \rightarrow Mn^{3+}$ substitution up to about $x_{M^{3+}} = 1.0$. This increasing bending of the Si_2O_7 group is expected when the larger M^{3+} ions, both Mn^{3+} and Fe^{3+} with $IR^{[6]} = 0.645$ Å (Shannon, 1976, high spin configurations), substitute for the smaller Al with $IR^{[6]} = 0.535$ Å, as is obvious from the topology of the clinozoisite structure type (Dollase, 1968). The data on $\bar{R}_{M-O}$ in M(3) and the bending angle of Si_2O_7 in the Fe^{3+}-bearing natural piemontite from Ultevis as well as in the high-iron epidote of Gabe et al. (1973) are significantly lower or higher, respectively, compared with the slope of the relations in Fig. 7. This might be a first indication that the structural influences of Mn^{3+} and Fe^{3+} are different.

To work out such eventually existing differences more clearly, increments of distance changes, $\Delta R_{M-O}/\Delta x_{M^{3+}}$, of the individual M(1)–O(i) and M(3)–O(i) distances were calculated in the piemontites studied as well as in piemontite from St. Marcel and, for comparison, in two epidotes. The data obtained are listed in Table 7. It should first be noted that all increments of the individual distance changes, M(1)–O(i) as well as M(3)–O(i) have positive values.

Table 7. Increments of distance changes, $\Delta R_{M-O}/\Delta x_{M^{3+}}$, in M(1) and M(3) octahedra of synthetic piemontites with $M^{3+} = Mn^{3+}$, and of natural piemontites with $M^{3+} = (Mn^{3+} + Fe^{3+})$ as calculated using data of Tables 5 and 6. The reference data for R_{M-O} at the site fraction of M^{3+}, $x_{M^{3+}} = 0.0$, are taken from clinozoisite (Dollase, 1968). No increments are given for M(2) as there are negligible $x_{M^{3+}}$ in this site (Table 5) and, as a consequence, $\Delta R_{M(2)-O}$ scatters within or close to the limit of error (Table 6). Increments were calculated and are included for piemontite from St. Marcel (Dallase, 1969) and also for two epidotes (Gabe et al., 1973), the latter to discover eventually existing differences between the effects of substituting Mn^{3+} and $(Mn^{3+} + Fe^{3+})$ on the clinozoisite structure type compared to Fe^{3+}.

M^{3+}		Synthetic piemontites			Natural piemontites			Epidotes (Gabe et al., 1973)	
		MK-35/8 Mn^{3+}	PF-66/14 Mn^{3+}	MK-42/1 Mn^{3+}	Lom Pie 1 ($Mn_{0.25}^{3+}Fe_{0.75}^{3+}$)	Ultevis PIULT-1 ($Mn_{0.57}^{3+}Fe_{0.43}^{3+}$)	St. Marcel (Dollase, 1969) ($Mn_{0.7}^{3+}Fe_{0.3}^{3+}$)	LEP Fe^{3+}	HEP Fe^{3+}
M(1)		$x_{M^{3+}} = 0.168$	$x_{M^{3+}} = 0.173$	$x_{M^{3+}} = 0.460$	–	$x_{M^{3+}} = 0.156$	$x_{M^{3+}} = 0.200$		
	M(1)–O(1) 2×	0.050	0.052	0.103	–	0.096	0.055	–	–
	M(1)–O(4) 2×	0.131	0.098	0.070	–	0.096	0.110	–	–
	M(1)–O(5) 2×	0.208	0.220	0.170	–	0.256	0.240	–	–
M(3)		$x_{M^{3+}} = 0.715$	$x_{M^{3+}} = 0.740$	$x_{M^{3+}} = 0.931$	$x_{M^{3+}} = 0.501$	$x_{M^{3+}} = 0.964$	$x_{M^{3+}} = 0.830$	$x_{M^{3+}} = 0.400$	$x_{M^{3+}} = 0.840$
	M(3)–O(1) 2×	0.128	0.115	0.100	0.076	0.076	0.108	0.040	0.048
	M(3)–O(2) 2×	0.132	0.126	0.130	0.095	0.095	0.127	0.076	0.071
	M(3)–O(4)	0.015	0.019	0.074	0.054	0.054	0.047	0.104	0.088
	M(3)–O(8)	0.060	0.069	0.070	0.088	0.088	0.096	0.073	0.094

When we now consider the data for the M(3) octahedron which incorporates by far the largest fraction of M^{3+}, it is obvious that the most prominent distance increase on increasing $x_{M^{3+}}$ occurs in M(3)–O(1) and –O(2) when $M^{3+} = Mn^{3+}$ or $(Mn_{1-n}^{3+}Fe_n^{3+})$. In the epidotes where $M^{3+} = Fe^{3+}$ exclusively, the increments of of distance changes do not differ as strongly as in piemontites (Table 7). Also, in epidotes the increments of M(3)–O(1) and M(3)–O(2) are lower than the others (Table 7), just opposite to the manganian phases. From Fig. 5, it is obvious that each two symmetrically equivalent atoms O(1) and O(2) form the "octahedral plane" of the compressed $M(3)O_6$ octahedron while O(4) and O(8) form the "octahedral apices". Thus, the increasing distance of M(3)–O(i) in the manganian phases causes an increasing size of this polyhedron but at the same time an increasing relative compression along O(8)M(3)O(4) with increasing $x_{Mn^{3+}(M(3))}$ which is not observed in epidote. These observations prove a distinct Jahn Teller effect of Mn^{3+} in piemontite M(3) octahedra. This effect is opposite to that observed in the andalusite structure type, where the elongation of the $M(1)O_6$ octahedron increases on increasing $Al \rightarrow Mn^{3+}$ in the manganian andalusite solid solution series (Abs-Wurmbach et al., 1981). Thus, in the compressed piemontite M(3) octahedra the electron hole of the d^4 – configurated Mn^{3+} occurs in the crystal field ground state of this ion in the d_{z^2} orbital while in the andalusite M(1) sites it exists in the $d_{(x^2-y^2)}$ orbital. This is a nice example of the axial inversion effect in Jahn-Teller distorted ML_6 octahedra which was already discussed by Strens (1966). The fact that the distance increment for M(3)–O(8) is definitely larger than that of M(3)–O(4) in the manganian minerals shows that on increasing Mn^{3+} M(3) site fraction the compression of the M(3) octahedra along their apical axes becomes similar (cf. Table 6 and Fig. 5), an effect which is also not observed for Fe^{3+} in the M(3) octahedra of epidotes. Instead, here the "asymmetry of the axial distortion" of the M(3) octahedra increases (Table 7).

In the $M(1)O_6$ octahedra, there exist as in the $M(3)O_6$ octahedra, four long and two short M–O distances, M(1)–O(1) and M(1)–O(5) or M(1)–O(4), respectively. Hence, the $M(1)O_6$ octahedra are also – at least in a first approximation – compressed, in this case with the octahedral axis of compression along O(4)M(1)O(4) (Table 6, Fig. 5). Their volume is smaller than that of the M(3) octahedra. As in the case of the latter, the relative compression of the M(1) octahedra increases on increasing Mn^{3+} population as is obvious from the decrease of the increment of distance change for the apical M(1)–O(4). Other than in the case of the M(3) octahedra, the distortion of the "octahedral plane" increases on increasing $x_{Mn^{3+}(M(1))}$, which is clear from the fact that the increment of distance change is highest for M(1)–O(5) among the three M(1)–O distances (Table 7).

Polarised electronic absorption spectra of natural and synthetic "thulites" and piemontites

The $\mathbf{E} \parallel \mathbf{X}(n_\alpha)$-, $\mathbf{E} \parallel \mathbf{Y}(n_\beta)$- and $\mathbf{E} \parallel \mathbf{Z}(n_\gamma)$-polarised electronic single crystal spectra in the spectral range 35000–5000 cm^{-1}, of "thulites" and piemontites and their synthetic equivalents obtained in this study on the crystals mentioned in Table 1 are presented in Figs. 1 and 8. The crystallographic orientation of the optical indicatrix axes, **X**, **Y** and **Z** are given in the section on methods as well as in Fig. 5. They were confirmed by the pleochroism of the crystals, their optical extinctions as well as conoscopic observations.

UV absorption edges:

The spectra of all piemontites, natural as well as synthetic ones, are dominated by a slightly polarised absorption edge in the UV. This absorption edge occurs at lower en-

ergies in natural than in synthetic crystals when comparing those with similar substitutional degree $p_{M^{3+}}$ (cf. e.g. spectra of synthetic piemontite with $p_{Mn^{3+}} = 0.83$ with those of the Andros piemontite with $p_{M^{3+}} = 0.87$). On increasing substitution $Al \rightarrow Mn^{3+}$, the edges shift to lower energies, most strongly in the case of **E** || **Y** (Fig. 9).

Spin-allowed dd bands of Mn^{3+} in M(3):

All spectra are further dominated by three intense and strongly polarised absorption bands ν_I, ν_{II} and ν_{III} (Table 8, upper part) with half band widths of up to 3000 cm^{-1}. These bands are typical spin allowed dd transitions of Mn^{3+} in the M(3) octahedra of the piemontite structure (Burns and Strens, 1967; Langer et al., 1976; Smith et al., 1982; cf. introduction). These three bands shift slightly to lower energies on increasing M(3) site fraction of Mn^{3+}, as displayed in the upper part of Fig. 10. The low energy shifts of ν_I, ν_{II} and ν_{III} and the derived decrease of the crystal field parameter 10 Dq of Mn^{3+} in M(3), in connection with distance data reported here, have been used to calculate the change of the local

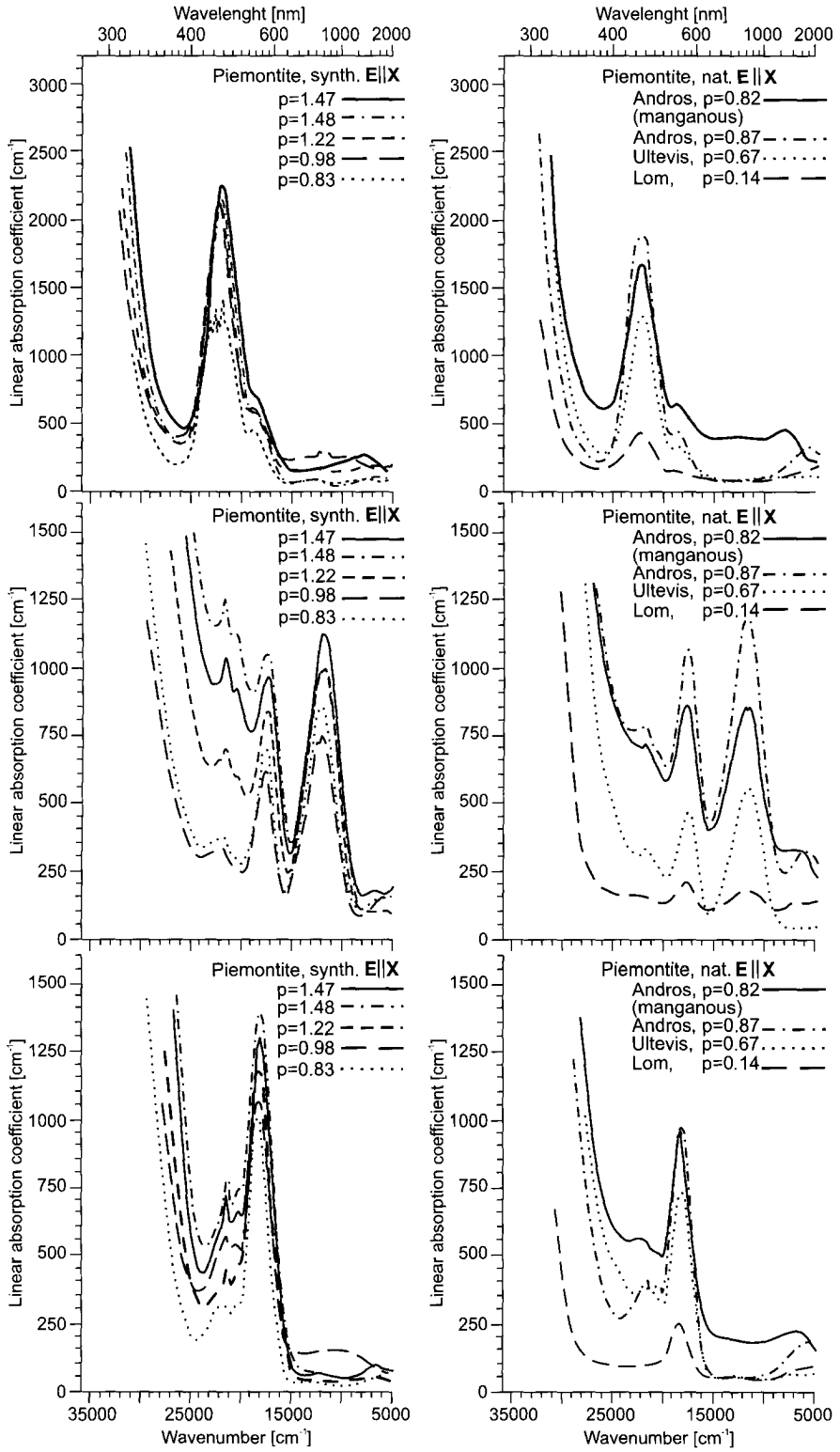

Fig. 8. Polarised single crystal absorption spectra **E** || **X** (≈ **c**), top, **E** || **Y**(|| **b**), middle, and **E** || **Z**(< **a** ≈ 30°), bottom, of synthetic (left) and natural (right) piemontites with different substitutional degrees. As all bands are caused by Mn^{3+}-transitions, the p-values quoted are the analysed manganese contents $Mn_{tot} = Mn^{3+}$ pfu (cf. Table 1). Note that the ordinates are thickness normalised linear absorption coefficients such that the intensities in the different spectra can directly be compared. Note also that the same ordinate scaling is used for **E** || **X** and **Z** while for **E** || **Y** the ordinate is expanded by a factor of two compared to the spectra with the two other polarisations. Thus, all spectra can be compared and evaluated in terms of band energies and also in terms of band intensities.

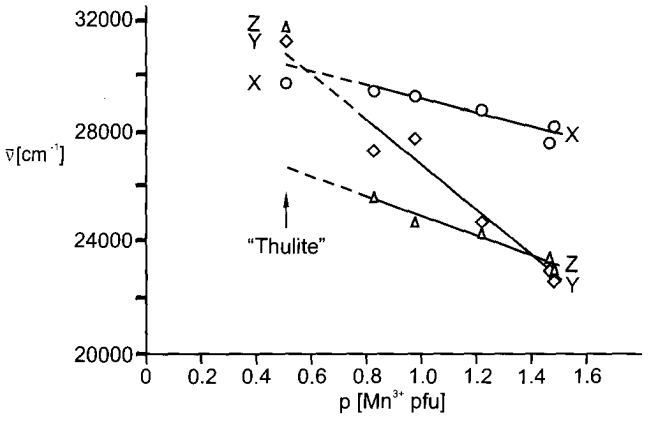

Fig. 9. Dependence of the energy of the absorption edge in the UV in the polarised spectra of the synthetic "thulite" and piemontites on the substitutional degree $p_{Mn^{3+}}$. The absorption edge is defined as the wavenumber at which the linear absorption coefficient is $\alpha = 1200\ cm^{-1}$ over the background (horizontal tangent to the minimum near $16000\ cm^{-1}$), i.e. where $T = 0.1\%$ for 25 μm thickness such that the crystal plate is opaque at thin section thickness. The same symbols as in Fig. 3 represent **X**, **Y**, **Z**.

mean octahedral distance in $M(3)O_6$ on decreasing $x_{Mn^{3+}(M3)}$ (Langer, 2001), which is found appreciably smaller than the "virtual" mean distances from the crystal averaging X-ray structure refinements (cf. Fig. 7).

As already stated, "thulites" also show the three strong Mn^{3+}(M3) bands ν_I, ν_{II}, and ν_{III}. However, their energies are significantly higher than expected from extrapolating the slopes of band energies with respect to $x_{Mn^{3+}}$ (Fig. 10, upper part). This is consistent with a significantly smaller $\bar{R}_{M(3)-O}$ in "thulite" compared to piemontite (Table 6).

Evaluation of the intensities of ν_I, ν_{II}, ν_{III} of Mn^{3+} in piemontite M(3) and Mn^{3+}–Fe^{3+} fractioning in the natural minerals:

The lower parts of Fig. 10 display the linear absorption coefficients, $\alpha[cm^{-1}] = \log(I_0/I)/t$, as a function of the site fractions $x_{Mn^{3+}(M3)}$ in the synthetic, pure Mn^{3+}-piemontites. The $\alpha_{I,\,II,\,III}$ are plotted for those polarisations where they have maximum value. The dashed lines in the lower part of Fig. 10 represent interpolations of the $\alpha_{I,\,II,\,III}$

Table 8. Energy and intensity ranges as well as polarisation of spin-allowed dd bands of Mn^{3+} in M(3) and M(1), as identified in synthetic piemontites (Table 1) in the spectral range 25000–10000 (cf. Fig. 8 and Text). The linear absorption coefficients, $\alpha = \log(I_0/I)/t$, are given in $[cm^{-1}]$; n.d. = not detected.

	Energy range $[cm^{-1}]$	Polarisation	Intensity range
Mn^{3+} (M3)			
ν_I	12000–13000	$\parallel$ **Y**	$\alpha_{I,\,Y} = 937.5 \cdot x_{Mn^{3+}(M3)}$
ν_{II}	18000–19000	$\parallel$ **Z** and **Y** (**Z** > **Y**)	$\alpha_{II,\,Z} = 2317.5 \cdot x_{Mn^{3+}(M3)}$
ν_{III}	22000–24000	$\parallel$ **X**	$\alpha_{III,\,X} = 2111 \cdot x_{Mn^{3+}(M3)}$
Mn^{3+} (M1)[a]			
ν_I	n.d.	n.d.	n.d.
ν_{II}	ca. 20000 (broad)	$\parallel$ **Y** and **Z** (**Y** ≈ **Z**)	
ν_{III}	21870–21590	$\parallel$ **Z** and **Y** (**Z** > **Y**)	$70 \le \alpha_Y \le 230$ $350 \le \alpha_Z \le 690$

a: Data from spectra of crystals with $0.83 < p_{Mn^{3+}} < 1.48$

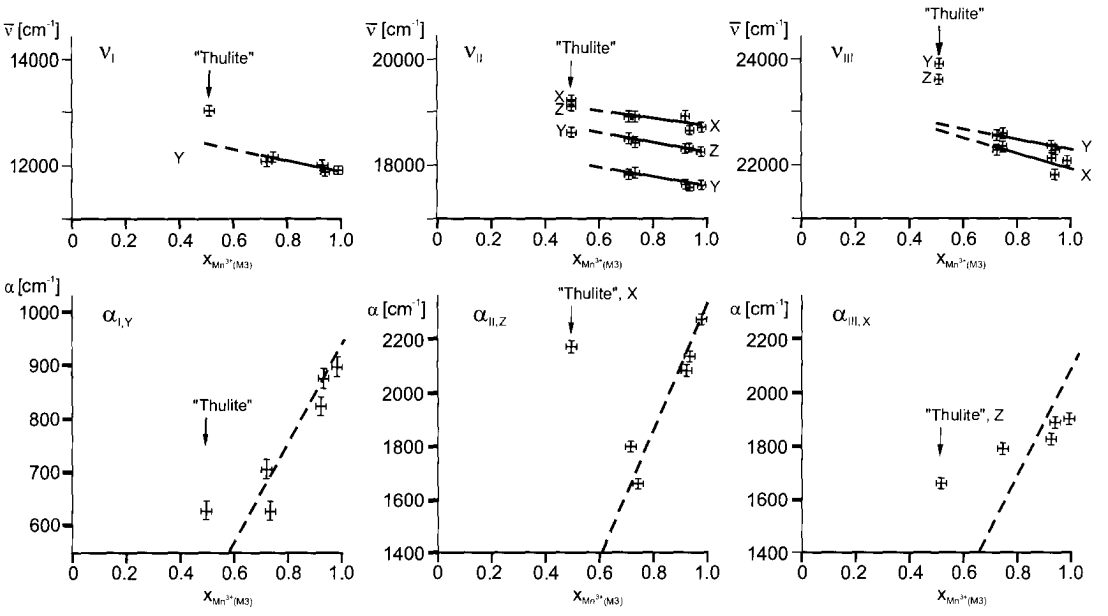

Fig. 10. Energy positions $\bar{\nu}$ (top) and linear absorption coefficients α (bottom) of spin-allowed Mn^{3+}M(3) dd-bands in polarised single crystal spectra of synthetic "thulite" and piemontites, in dependence of the site fraction of trivalent manganese in M(3), $x_{Mn^{3+}(M3)}$ (cf. text). Sizes of crosses represent the experimental errors.

Table 9. Experimental and calculated intensities, α [cm^{-1}], of spin-allowed Mn^{3+} (M3) dd-bands in natural piemontites. The calculated data are obtained using the $\alpha_{I,II,III} = f(x_{Mn^{3+}(M3)})$ relations of Table 8, for two models of the intracrystalline Mn^{3+} distribution: (1) Mn^{3+} in M(3) only, (2) the distribution of Mn^{3+} between M(3) and M(1) is the same as that of Fe^{3+} (cf. Text). The experimental α-values are subject to uncertainties of about 5%, mainly due to uncertainties of thickness measurements of the crystal platelets.

	Piemontite Lom			Piemontite Ultevis			Piemontite Andros (AND 79–183)		
	α_{exp}	$\alpha_{calc(1)}$	$\alpha_{calc(2)}$	α_{exp}	$\alpha_{calc(1)}$	$\alpha_{calc(2)}$	α_{exp}	$\alpha_{calc(1)}$	$\alpha_{calc(2)}$
$\alpha_{I,Y}$	140	134	120	500	619	440	833	630	572
$\alpha_{II,Z}$	370	331	289	1100	1530	1089	1670	1550	1413
$\alpha_{III,X}$	280	302	264	1110	1390	992	1730	1410	1288

$= f(x_{Mn^{3+}(M3)})$ functions assuming linear Beer-functions with $\alpha_{I,II,III} = 0\ cm^{-1}$ for $x_{Mn^{3+}(M3)} = 0$. Table 8 summarises the functions obtained together with other properties of the spin-allowed dd-bands of Mn^{3+}(M3) in piemontite. The α-values of "thulite" are again distinctly higher than expected from the extrapolations of the piemontite functions (Fig. 10, bottom). The reason may be that the distortion of the $M(3)O_6$ octahedra which in both minerals have site symmetry m, in "thulite" differs significantly from that in piemontite:

piemontite, PF66: $\lambda_{oct} = 1.0349$, $\sigma_{oct}^2 = 83.7$

"thulite", Lom: $\lambda_{oct} = 1.0211$, $\sigma_{oct}^2 = 29.1$

using the mean quadratic elongation, λ_{oct}, and the bond angle variance, σ_{oct}^2, as defined by Robinson et al. (1971) and the structural data of the present work.

The relations $\alpha_{I,II,III} = f(x_{Mn^{3+}(M3)})$ presented in Table 8, last column, can be used to obtain information about the Mn^{3+}–Fe^{3+} fractionation in the intracrystalline distribution in piemontites from Lom, Ultevis and Andros (AND79-183): All of these are characterised by substitutional degrees $p_{M^{3+}} < 1.00$. Hence, the capability of the relations in Table 8 to contribute to the solution of the just mentioned fractionation problem can be demonstrated by calculating the α-values to be expected for two models of Mn^{3+}–Fe^{3+} fractionation, and compare them with the experimental data. The models are:

(1) All Mn^{3+} present (Table 4) is allocated in M(3), i.e. $x_{Mn^{3+}} = p_{Mn^{3+}tot}$. The deficit compared with $x_{(Mn^{3+}+Al+Fe^{3+})} = 1.00$ is Fe^{3+} which implies that Fe^{3+} fractionates predominantly in M(1), Mn^{3+} into M(3).

(2) Mn^{3+} and Fe^{3+} do not fractionate but behave in the same manner in the M(3)–M(1) intracrystalline distribution such that $x_{Mn^{3+}(M3)} = p_{M^{3+}tot}(x_{M^{3+}(M3)}/x_{M^{3+}tot})$.

The comparison of the experimental data with those calculated for these two models is presented in Table 9 and clearly shows that the distribution behaviour of Mn^{3+} and Fe^{3+} between M(3) and M(1) is not the same and that the former dominates the latter with respect to allocation in M(3). This is the case in principle for all three natural piemontites though less clearly for the Ultevis sample.

One might think that Mössbauer spectroscopy could help to solve the fractionation problem. However, difficulties in resolving the spectra did not allow for unequivocal conclusions (F. Seifert, personal communication).

Table 10. Polarisation of spin-allowed Mn^{3+} (M3) dd bands as calculated on the basis of the energy level diagram for $C_{2v}(C_2'')$ point symmetry shown in Fig. 11, compared to the observed polarisations in spectra of synthetic piemontites. The fair correspondence of calculated and observed values proves the applicability of the energy level diagram in Fig. 11.

		α_X : α_Y : α_Z
Calculated		
	ν_I	0 : 1 : 0
	ν_{II}	0 : 0 : 1
	ν_{III}	1 : 0 : 0
Observed		
MK-35, $p_{Mn^{3+}} = 0.83$	ν_I	0.03 : 1 : 0.01
	ν_{II}	0.20 : 0.27 : 1
	ν_{III}	– – – – –
PF-66, $p_{Mn^{3+}} = 0.98$	ν_I	0 : 1 : 0
	ν_{II}	0.20 : 0.26 : 1
	ν_{III}	1 : 0.03 : 0.21
MK-37, $p_{Mn^{3+}} = 1.22$	ν_I	0 : 1 : 0
	ν_{II}	0.21 : 0.24 : 1
	ν_{III}	1 : 0.03 : 0.11
MK-42, $p_{Mn^{3+}} = 1.47$	ν_I	0 : 1 : 0
	ν_{II}	0.20 : 0.23 : 1
	ν_{III}	1 : 0.04 : 0.21
MK-41, $p_{Mn^{3+}} = 1.48$	ν_I	0 : 1 : 0
	ν_{II}	0.19 : 0.21 : 1
	ν_{III}	1 : 0 : 0.16

Evaluation of the energies of the spin-allowed bands ν_I, ν_{II} and ν_{III} of Mn^{3+} in M(3) – crystal field stabilisation:

In the theoretical evaluation of the three spin-allowed bands of Mn^{3+} in M(3) with point symmetry *m*, it is first to be stated that the nearly complete polarisation of bands ν_I, ν_{II} and ν_{III} along the optical **Y**, **Z** and **X** directions, respectively, i.e. approximately along one of the internal axes of the M(3) octahedron (cf. Fig. 5), cannot be interpreted on the basis of the point group m. Hence, a supergroup of C_s is to be found which allows for three spin allowed bands and their observed polarisations.

This supergroup should, like C_s does, lack an inversion center and should be a subgroup of D_{4h} because the M(3) polyhedron is in a first approximation an octahedron compressed along one of the tetrad axes (Burns and Strens, 1967, Langer, et al. 1976, Smith et al., 1982). Group theoretical calculations with the application of the correlation tables of Wilson et al. (1955), of the direct products $\Gamma\Psi_g \cdot P_{x,y,z} \cdot \Gamma\Psi_a{}^*$ (Marfunin, 1979) show that the point group $C_{2v}(C_2'')$ is best suited to interpret the number and

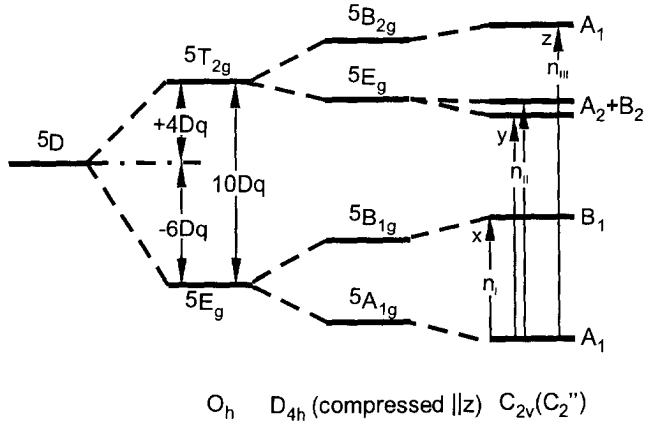

Fig. 11. Schematic energy level diagram of $3d^4$-configurated Mn^{3+} in axially compressed octahedral coordination of descending symmetry. The crystal field splitting for true regular symmetry O_h and the irreducible representations of terms in O_h are shown as if the octahedra were already compressed along the four-fold axis to keep the scheme simple. The polarisations of the symmetry allowed transitions as calculated using group theoretical methods and given for the pseudosymmetry $C_{2v}(C_2'')$, refer to the internal axes of $[M(3)O_6]$ in this point group. Their relations to the crystallographic axes and the principal optical directions **X**, **Y** and **Z** are shown in Fig. 5.

polarisations of the observed bands. Fig. 5 includes the internal octahedral axes x_{oct}, y_{oct} and z_{oct} in this point group. The diad axis is parallel to z_{oct} and the vertical mirror plane is perpendicular to the plane 2O(1)–2O(2). The directions of the optical indicatrix axes relative to the internal octahedral axes are $\mathbf{X} \parallel \approx z_{oct}$, $\mathbf{Y} \parallel x_{oct}$ and $\mathbf{Z} \parallel \approx y_{oct}$ (Fig. 5). The above mentioned group theoretical deductions yield the energy level diagram for $C_{2v}(C_2'')$ shown in Fig. 11. The number of observed bands and their polarisations are well in accord with the selected pseudosymmetry. This is also obvious from Table 10, summarising calculated and experimental intensity ratios for bands ν_I, ν_{II} and ν_{III} of the five synthetic piemontites. Thus, the energy level diagram obtained for the pseudosymmetry $C_{2v}(C_2'')$ shown in Fig. 11 is basically correct for Mn^{3+} in M(3) sites of the clinozoisite structure type. Effects of spin-orbit coupling and of interactions between terms with the same irreducible representations are not shown in Fig. 11. These will be integral parts of the experimentally determined energy values E_I, E_{II} and E_{III} of the respective transitions. Thus, the octahedral crystal field parameter 10 Dq can be calculated by

$$10\,Dq_{oct} = E_{III} - 2(E_{III} - E_{II})/3 - E_I/2$$

as is obvious from Fig. 11. Here, E_I is the ground state spitting δ caused by the Jahn-Teller effect of Mn^{3+} in the compressed M(3) polyhedra of the clinozoisite structure type. The octahedral crystal field stabilisation energy of the $3d^4$-configurated Mn^{3+}-ion in M(3) is then

$$CFSE_{Mn^{3+}(M3)} = -(6\,Dq_{oct} + \delta/2)\,.$$

The values obtained for $10\,Dq_{oct}$ and CFSE of Mn^{3+} in piemontite M(3) are listed in Table 11, the Jahn-Teller splitting δ can be taken from Fig. 10 (upper part, left). The crystal field splitting and crystal field stabilisation energy of Mn^{3+}(M3) decrease slightly on increasing M(3) site fraction of Mn^{3+}, $CFSE_{Mn^{3+}}$ by $-200\ cm^{-1}$ per $0.1\ x_{Mn^{3+}(M3)}$ in the range between MK35 and MK42 (cf. Table 11). The difference in $CFSE_{Mn^{3+}}$ per $0.1\ x_{Mn^{3+}(M3)}$ between "thulite" MK25 and piemontite MK35 amounts to only $-90\ cm^{-1}$ per $0.1\ x_{Mn^{3+}(M3)}$.

Spin-allowed dd bands of Mn^{3+} in M(1):

According to the results of the structure determinations, significant amounts of Mn_{tot}^{3+} substitute for Al in M(1) even when the total substitutional degree $p_{Mn^{3+}tot}$ is below 1.0, and increases strongly – up to 0.46 (MK42, Table 5) – when $p_{Mn^{3+}tot} \geq 1.0$ (Fig. 6). Hence, bands caused by Mn^{3+}(M1) are expected to be detectable as the shape of the spectra should gradually change in the respective spectral regions with increasing site fraction of Mn^{3+}(M1). However, it must be borne in mind that the specific intensities of bands originating from Mn^{3+}(M1) will be much smaller than those of Mn^{3+}(M3) because M(1) is centrosymmetric, and M(3) not. In this latter case, the Laporte selection rule of spin-allowed dd transitions is at least partly lifted. The ratios of intensities may be 1:10 or more in such a case. In search of Mn^{3+}(M1) bands, it is further worth to recall that the M(1) polyhedra can be considered as compressed polyhedra as this is the case for the M(3) polyhedra. Hence, Mn^{3+}(M1) should exhibit three spin-allowed bands, ν_I, ν_{II} and ν_{III}, as Mn^{3+}(M3) does (Fig. 11). These bands are expected at higher energies than the corresponding bands of Mn^{3+}(M3), as M(1) polyhedra have a

Table 11. Crystal field parameter 10 Dq as calculated from energies of spin-allowed Mn^{3+} (M3) dd bands on the basis of the energy level diagram of Fig. 11 and crystal field stabilisation energy, $CFSE_{Mn^{3+}(M3)}$ in synthetic piemontites and "thulite".

	$p = Mn^{3+}{}_{pfu}$	$x_{Mn^{3+}(M3)}$	$10\,Dq^a$ [cm^{-1}]	$CFSE_{Mn^{3+}}$ [cm^{-1}]	[KJ/g-atom]$_{Mn}$
"Thulite"					
MK-25	0.51	ca. 0.51	13780	−14790	−176.9
Piemontite					
MK-35	0.83	0.715	13600	−14510	−173.5
PF-66	0.98	0.74	13620	−14260	−170.6
MK-37	1.22	0.93[b]	13570	−14170	−169.5
MK-42	1.47	0.931	13540	−14080	−168.5
MK-41	1.48	0.96[b]	13530	−14090	−168.5

a: Energies of ν_I ν_{II} and ν_{III} were obtained as averages over the values in the three polarisation directions in the calculation of 10 Dq

b: Interpolated using the distribution diagram of Fig. 6

smaller mean M–O distance and, therefore, $10\,Dq_{Mn^{3+}}$ is higher in M(1) than in M(3) polyhedra at the same site fractions. This is obvious when we compare the mean distances in M(3)–O in piemontite from Lom with those of M(1)–O in MK42. On the basis of these considerations, it is obvious that the energy ranges above 19000 cm^{-1} of the $\mathbf{E} \parallel \mathbf{Y}$ and $\mathbf{E} \parallel \mathbf{Z}$ spectra do indeed display bands in addition to those of Mn^{3+}(M3) which fit the above requirements, while in $\mathbf{E} \parallel \mathbf{X}$, they are superimposed by the very strong ν_{III} band of Mn^{3+}(M3) (Fig. 8). Thus bands originating from Mn^{3+}(M1) are possibly:

	$\mathbf{E} \parallel \mathbf{X}$	$\mathbf{E} \parallel \mathbf{Y}$	$\mathbf{E} \parallel \mathbf{Z}$	
ν_I	?	?		
ν_{II}	?	ca. 20000	ca. 20000	(broad)
		$\alpha_Y < \alpha_Z$		
ν_{III}	?	21820–21630	21870–21590	
		α 70–230	α 350–690	(narrow)

The numbers given here for the inferred bands of Mn^{3+} in M(1) are taken from direct inspection of the spectra. Attempts to improve such results by curve analyses of the spectra failed because of the very complicated shape of the spectra which allowed for a large number of fitting models which met the observed spectral shape equally well.

Spin-forbidden dd-bands of Mn^{3+}

show up as distinct, sharp and weak bands or shoulders near 20000 and 21500 cm^{-1} in piemontites (Fig. 8) and near 20000 cm^{-1} in "thulites" (Fig. 1). Their energies are compatible with those expected for transitions to excited crystal field states of Mn^{3+} derived from ^3P, ^3H, ^3F and ^3G (Marfunin,1979; König and Kremer, 1977)

$Mn^{2+}Mn^{3+}$ charge-transfer?

Calculations of the chemical formulae of the minerals studied (Table 4) showed that piemontite AND79–255 from Andros, holds significant amounts of manganese as Mn^{2+}, substituting for calcium on the (A1, A2) sites of the structure. According to the data in Table 4, about 10% of calcium is substituted. Thus, the question arises whether the spectra of this piemontite might show the above homonuclear MM-CT which may be expected to occur near 18600 and 25400 cm^{-1}, when results on purple yoderite are considered (Langer et al., 1982).

Comparing spectra of the Mn^{2+}–Mn^{3+}-bearing Andros piemontite AND79–255 with those of the Ultevis sample (Fig. 8) shows that the former displays indeed a distinctly different shape in the 23000 cm^{-1} range for $\mathbf{E} \parallel \mathbf{Z}$. On the other hand, any Mn^{2+}(A1, A2)–Mn^{3+}(M3) charge-transfer transitions should occur approximately along $\mathbf{X}$ because of the orientation of the respective (A1, A2)–M(3) vectors. Thus, it remains unclear whether the above mentioned spectral peculiarities are really caused by homonuclear manganese charge transfer.

Spectral features in the NIR below about 8000 cm^{-1}

occur as broad and weak band- or minima-like shapes in spectra of natural as well as synthetic crystals. These features are not specific of any electronic transition of either Mn^{3+}- or Fe^{3+}-ions. They are rather caused by diffraction- and refraction-related effects in the NIR region, typical of small crystals, embedded in a resin with lower refractive index (Langer and Abu-Eid, 1977).

Conclusions – Jahn-Teller effect of Mn^{3+} and octahedral axial inversion

On the basis of six new structure refinements and eleven full sets, $\mathbf{E} \parallel \mathbf{X}$, $\mathbf{Y}$ or $\mathbf{Z}$, of polarised single-crystal electronic absorption spectra in the energy range 35000–5000 cm^{-1} (4.34–0.62 eV) on 11 natural and synthetic orthozoisite-type "thulites" and clinozoisite-type piemontites (Table 1), $Ca_2(Al_{3-p}M_p^{3+})[OH \mid O \mid SiO_4 \mid Si_2O_7]$ with $M^{3+} = Mn^{3+}$ or $(Mn_{1-n}^{3+}Fe_n^{3+})$ for synthetic or natural minerals, respectively, the following conclusions can be drawn:

It is demonstrated that Mn in "thulite" is in the trivalent state, like in piemontite. In both structure types, the trivalent transition-metal cations partition preferentially into the M(3) site. The M(2) octahedra, carrying the protons, are not involved in this partitioning process. The M(3) site preference of Mn^{3+} is stronger than that of Fe^{3+} in natural piemontites with $M^{3+} = (Mn_{1-n}^{3+}Fe_n^{3+})$. This is in accord with the Jahn-Teller effect of the $3d^4$-configurated Mn^{3+} in the axially compressed M(3) octahedra, which is absent in the spherically symmetrical $3d^5$-configurated Fe^{3+}.

The most prominent changes in the clinozoisite structure type with increasing $Al \rightarrow M^{3+}$ substitution are a strong increase of the mean cation-anion distances in the $[M(3)O_6]$ and $[M(1)O_6]$ octahedra with nearly the same slopes of +0.47% or +0.53% per $0.1x_{M^{3+}}$, respectively. Such increases in the mean distances are to be interpreted as fractional sums of the respective Al- and M^{3+}-centered M(3) or M(1) polyhedra (Langer, 2001).

The bending angle of the Si_2O_7-group in cis-configuration, $\sphericalangle$Si(1)–O(9)–Si(2), strongly decreases from 164.4° in clinozoisite (Dollase, 1968) to 147.4 in the most Mn-rich synthetic piemontite, MK-42–1, with $p_{Mn^{3+}} = 1.47$. Considering the topology of the clinozoisite structure type (Dollase, 1968), this is the consequence of the strongly preferred partioning of the large M^{3+} into M(3).

Evaluation of the changes of individual M–O bond lengths with increasing M^{3+} substitution in terms of increments of distance changes, $\Delta R_{(M-O)i}/x_{M^{3+}}$ with $x_{M^{3+}}$ = site fraction of the Al-substituting M^{3+} (Table 7), shows that as a consequence of raising $Al \rightarrow M^{3+}$ substitution, the relative axial compression of the M(3) octahedra increases. This effect is stronger for pure Mn substitutions in synthetic minerals than in natural Fe,Mn-piemontites. Such an effect does not occur on increasing $Al \rightarrow Fe^{3+}$ substitution in epidotes, as is obvious from the data of Gabe et al. (1973). These observations prove again the Jahn-Teller effect of Mn^{3+} in piemontite. Increasing relative compression of the Mn^{3+}-centered octahedra is opposite to what happens to the M(1) octahedra in the andalusite structure type with increasing $Al \rightarrow Mn^{3+}$ substitution in manganian andalusites where the relative axial elongation be-

comes stronger (Abs-Wurmbach et al., 1981). Both effects may result as a consequence of the Jahn-Teller theorem; the first one when the electron hole of $3d^4$ occurs in the d_{z^2} orbital and the second one when it is in the $d_{(x^2-y^2)}$ orbital. Both are related by the axial inversion effect (Strens, 1966).

Three intense and strongly polarised absorption bands ν_I at 12000–13000 (**Y**), ν_{II} at 18000–19000 (**Z** and **Y**) and ν_{III} at 22000–24000 (**X**) cm^{-1} are correlated in energy and intensity with the M(3) site fraction of Mn^{3+} and are, therefore, to be assigned to spin-allowed dd-transitions of this cation in such sites lacking an inversion centre. The polarisation behaviour of the ν_I to ν_{III} bands is well understood assuming a pseudo-symmetry $C_{2v}(C_2'')$of the M(3) sites (Fig. 11, Table 10). From this, we obtain an octahedral crystal field parameter of 10 Dq = 13530 cm^{-1} when the M(3)-sites are nearly completely occupied by Mn^{3+}, $x_{Mn^{3+}(M3)} = 0.96$, in MK41 (cf. Table 11). This is a smaller 10 Dq value than that in andalusite-kanonaite solid solutions, "viridines" (14300 cm^{-1} for $x_{Mn^{3+}(M1)} = 0.72$; Abs-Wurmbach et al., 1981). Lowering the M(3) site occupancy of Mn^{3+} in piemontite enhances 10 Dq slightly (Table 11). The corresponding increase of 10 Dq in "viridines" is stronger (Abs-Wurmbach et al., 1981). On the other hand, the Jahn-Teller splitting, δ, of the ^5E_g crystal-field ground state of Mn^{3+} decreases strongly with decreasing $x_{Mn^{3+}(M3)}$ in "viridine", while in piemontite δ increases slightly with decreasing $x_{Mn^{3+}(M3)}$ (Fig. 10, ν_I).

Such crystal field data and their dependencies on the site fractions of Mn^{3+} lead to different crystal field stabilisation energies of this cation in the two structure types. With the highest Mn^{3+} site fractions attained in piemontite, i.e $x_{Mn^{3+}(M3)} = 0.96$, or kanonaite, i.e. $x_{Mn^{3+}(M1)} = 0.72$, $CFSE_{Mn^{3+}}$ amounts to 14090 cm^{-1} or 16600 cm^{-1}, respectively. In piemontite, it increases slightly with decreasing site fraction, by 28 cm^{-1} per $-0.1x_{Mn^{3+}(M3)}$, while in manganian andalusite it remains nearly constant in the entire substitutional range. To understand this different behaviour of Mn^{3+}, we compare the relative axial distortions of the compressed $M(3)O_6$- and elongated $M(1)O_6$-octahedra in piemontite and manganian andalusite, respectively, both with the same Mn^{3+}-site fractions (i.e. synthetic piemontite MK-35 with $x_{Mn^{3+}(M3)} = 0.715$ and kanonaite with $x_{Mn^{3+}(M1)} = 0.72$). To compare these two minerals, we calculate $(c/a)_{oct,M(3)} = 0.861$ in the former and $(c/a)_{oct,M(1)} = 1.190$ in the latter. When we now compare such values with the respective $(c/a)_{oct}$ values for the corresponding Mn^{3+}-free Al-end members, 0.880 in clinozoisite (for $M(3)O_6$ with data from Dollase, 1968) or 1.120 in andalusite (for $M(1)O_6$ with data from Burnham and Buerger, 1961), it is evident that the same Mn^{3+} site fraction enhances the axial octahedral compression of the M(3) site in clinozoisite by 2.2%, while for the M(1) site in andalusite the axial elongation increases by 6.3%. Such differences as well as the axial inversion may count for the different crystal chemical behaviour of Mn^{3+} in the clinozoisite and andalusite structure types.

No clear decision can be made for the spin-allowed dd bands of Mn^{3+} in the compressed M(1) octahedra of the clinozoisite type although about half of these polyhedra in the most Mn^{3+}-rich synthetic piemontites are occupied by Mn^{3+} (Fig. 6). The reasons are strong band overlap in the complex spectra (Fig. 8) and low intensities of the Mn^{3+}(M1)-bands due to the centrosymmetry of the M(1) site. Presumably, two bands at ≈20000 cm^{-1} (broad, ||**Y** and **Z**) and at 21870–21590 cm^{-1} (narrow, **Z** > **Y**) are the ν_{II} and ν_{III} bands of Mn^{3+} as they strongly gain intensity on increasing Mn^{3+}M(1) site fraction.

Although one of the natural piemontites (AND79–255) contains divalent Mn substituting for about 10% of the Ca in the (A1,A2) sites, no Mn^{2+}–Mn^{3+} charge transfer band, which should be strongly polarised parallel **c** (i.e. closely parallel to the optical **X** direction) could be identified with certainty in the spectrum of this peculiar piemontite.

Acknowledgments. The piemontite samples from Andros and Ultevis were kindly provided by Th. Reinicke, Bochum, and U. Hålenius, Stockholm, respectively, the synthesis product containing the piemontite crystals PF-66 by K.-R. Frentrup, Holderbank. The structure refinement of the piemontite from Ultevis was obtained through cooperation with S. Ghose, Seattle, its microprobe analysis by B. Evans, Seattle, during a research stay of K. L. in their laboratory. F. Seifert, Bayreuth, kindly measured Mössbauer-spectra on the piemontites from Ultevis and Lom and provided the data as a personal communication. S. Galbert, Berlin, helped with the microprobe analyses, S. Freitag, Berlin, in crystal orientation, by means of X-ray diffraction methods. H. Reuff, Berlin, prepared the thin slices of the oriented, minute crystals. The piston-cylinder apparatus of the high-pressure laboratory at the TU Berlin was maintained by M. Hellwig † and later by H. Winkelmann. The drawings and tables were carefully prepared by W. Zirbs, Vienna. The comments of two anonymous reviewers improved the manuscript, A. Woodland, Frankfurt, checked and improved the English text. The funds to start and carry out the project were provided by the Deutsche Forschungsgemeinschaft, Bonn, under grant number La 324/22-1 to 4. The Dean of the Faculty of Natural Sciences and Mathematics provided a travel grant for a stay of K. L. in Vienna. To all these persons and institutions our sincere thanks are due.

References

Abs-Wurmbach, I.; Langer, K.; Seifert, F.; Tillmanns, E.: The crystal chemistry of (Mn^{3+}, Fe^{3+})-substituted andalusites (manganian andalusites and kanonaite), $(Al_{1-x-y}Mn_x^{3+}Fe_y^{3+})_2[O\,|\,SiO_4]$: Crystal structure refinements, Moessbauer, and polarized optical absorption spectra. Z. Kristallogr. **155** (1981) 81–113.

Abs-Wurmbach, I; Langer, K.; Schreyer, W.: The influence of Mn^{3+} on the stability relations of the Al_2SiO_5 polymorphs with special emphasis on manganian andalusites (viridines), $(Al_{1-x}Mn_x^{3+})_2[O\,|\,SiO_4]$: An experimental investigation. J. Petrology **24** (1983) 48–75.

Anastasiou, P.; Langer, K.: Synthesis and physical properties of piemontite $Ca_2Al_{3-p}Mn_p^{3+}(Si_2O_7\,|\,SiO_4\,|\,O\,|\,OH)$. Contrib. Mineral. Petrol. **60** (1977) 225–245.

Baur, W. H.; Wenninger, G.; Roy, S.: SADIAN86. Universität Frankfurt 1986.

Burnham, C. W.; Buerger, M. J.: Refinement of the crystal structure of andalusite. Z. Kristallogr. **115** (1961) 269–290.

Burns, R. G.; Strens, R. G. J.: Structural interpretation of polarized absorption spectra of the Al-Fe-Mn-Cr epidotes. Mineral. Mag. **36** (1967) 204–226.

Cemič, L.; Geiger, C. A.; Hoyer, W. W.; Koch-Müller, M.; Langer, K.: Piston-cylinder techniques: Pressure and temperature calibration of a pyrophyllite-based assembly by means of DTA measurements, a salt-based assembly, and a cold-sealing sample encapsulation method. N. Jb. Miner. Mh. (1990) 49–64.

Chinner, G. A.; Smith, J. V; Knowles, C. R.: Transition metal contents of Al_2SiO_5 polymorphs. Am. J. Sci. Schairer Vol **267-A** (1969) 96–113.

Dollase, W. A.: Refinement and comparison of the structures of zoisite and clinozoisite. Am. Mineral. **53** (1968) 1882–1898

Dollase, W. A.: Crystal structure and cation ordering in piemontite. Am. Mineral. **54** (1969) 710–717.

Finger, L. W.; Prince, R.: US Natl. Bur. Stand., Techn Note **854** (1975).

Frentrup, K. R.; Langer, K.: Mn^{3-} in garnets: Optical absorption spectrum of a synthetic Mn^{3+} bearing silicate garnet. N. Jb. Miner. Mh. (1981) 245–256.

Frentrup, K. R.; Langer, K.: Microscope absorption spectrometry of silicate micro-crystals in the range 40000–5000 cm^{-1} and its application to garnet end members synthesized at high pressures. In: Schreyer, W. ed.: High-pressure researches in geosciences, pp 247–258. Schweizerbart, Stuttgart 1982.

Gabe, E. J.; Portheine, J. C.; Whitlow, S. H.: A reinvestigation of the epidote structure: Confirmation of the iron location. Am. Mineral. **58** (1973) 218–223.

International Tables for X-ray Crystallography, Vol. IV, revised and supplementary tables (Eds. J. A. Ibers, W. C. Hamilton) The Kynoch press, Birmingham 1974.

Jahn, H. A.; Teller, E.: Stability of polyatomic molecules in degenerate electronic ground states. I. Orbital degeneracy. Proc. Roy. Phys. Soc. (London) **A161** (1937) 220–235.

Kersten, M.; Langer, K.; Almen, H.; Tillmanns, E.: The polarized single crystal spectra and structures of synthetic "thulite" and piemontites, $Ca_2Al_{3-p}Mn_p^{3+}[OH\,|\,O\,|\,SiO_4\,|\,Si_2O_7]$ with $0.5 \leq p \leq 1.6$. Z. Kristallogr. **185** (1988) 111.

Keskinen, M.; Liou, J. G.: Stability relations of Fe–Mn–Al piemontite. J. Metamorph. Geol. **5**(4) (1987) 495–507.

König, E.; Kremer, S.: Ligand field energy diagrams. Plenum Press, New York 1977.

Langer, K.: UV to NIR spectra of silicate minerals obtained by microscope spectrometry and their use in mineral thermodynamics and kinetics. in: Salje, E. K. H. ed.: Physical Properties and Thermodynamic Behaviour of Minerals, pp. 639–685. Reidel, Dordrecht 1988.

Langer, K.: A note on mean distances, $\bar{R}_{[MO^6]}$, in substituted polyhedra, $[(M_{1-x}M_x')O_6]$, in the crystal structures of oxygen based solid solutions: local versus crystal averaging methods. Z. Kristallogr. **216** (2001) 87–91.

Langer, K.; Abu-Eid, R. M.: Measurement of the polarized absorption spectra of synthetic transition metal-bearing silicate microcrystals in the spectral range 44000–4000 cm^{-1}. Phys. Chem. Minerals **1** (1977) 273–299.

Langer, K.; Abu-Eid, R. M.; Anastasiou, P.: Absorptionsspektren synthetischer Piemontite in den Bereichen 43,000–4,000 cm-1 (232.6–909.1 nm) und 4000–250 cm^{-1} (2.5–40 μm). Z. Kristallogr. **144** (1976) 434–436.

Langer, K.; Smith, G.; Hålenius, U.: Reassignment of the absorption spectra of purple yoderite. Phys. Chem. Minerals **8** (1982) 143–145.

Marfunin, A. S.: Physics of Minerals and Inorganic Materials. Springer, Heidelberg 1979.

Robinson, K.; Gibbs, G. V.; Ribbe, P. H.: Quadratic elongation: A quantitative measure of distortion in coordination polyhedra. Science **172** (1971) 567–570.

Sheldrick, G.: Programs for crystal structure determination. Cambridge 1976.

Shannon, R. D: Revised effective ionic radii and systematic studies of interatomic distances in halides and chalcogenides. Acta Crystallogr. **A32** (1976) 751–767.

Smith, G.; Hålenius, U; Langer, K.: Low temperature spectral studies of Mn^{3+}-bearing andalusite and epidote type minerals. Phys. Chem. Minerals **8** (1982) 138–147.

Strens, R. G. J.: The axial-ratio-inversion effect in Jahn-Teller distorted ML_6 octahedra in the epidote and perovskite structures. Mineral. Mag. **35** (1966) 777–780.

Strunz, H.: Klockmanns Lehrbuch der Mineralogie, pp. 698–699. Enke Verlag, Stuttgart 1978.

Tillmanns, E.; Langer, K.; Arni, R.; Abraham, K.: Crystal structure refinements of co-existing thulite and piemontite, $Ca_2Al_{3-p}M_p^{3+}[OH\,|\,O\,|\,SiO_4\,|\,Si_2O_7]$ ($M^{3+} = Mn^{3+} + Fe^{3+}$). Thirteenth Int. Congr. Crystallogr., Hamburg (1984), Abstr 08.4–42.

Tröger, W. E.: Tabellen der gesteinsbildenden Minerale. Schweizerbart, Stuttgart 1952.

Wilson, E. B.; Decius, J. C.; Cross, P. C.: Molecular vibrations. McGraw Hill, New York 1955.